

UNIVERSITY OF HELSINKI

REPORT SERIES IN PHYSICS

HU-P-D276

Radiation Damage in High Entropy Alloys

Emil Levo

Division of Materials Physics
Department of Physics

Faculty of Science
University of Helsinki
Helsinki, Finland

DOCTORAL DISSERTATION

To be presented for public discussion with the permission of the Faculty of Science of the University of Helsinki, in Auditorium PIII, Porthania Building, on the 8th of January, 2022 at 10 o'clock

HELSINKI 2021

Supervisors

Doctor	Fredric Granberg <i>University of Helsinki, Department of Physics</i>
Professor	Kai Nordlund <i>University of Helsinki, Department of Physics</i>
Professor	Flyura Djurabekova <i>University of Helsinki, Department of Physics</i> <i>Helsinki Institute of Physics</i>

Pre-examiners

Professor	Matti Alatalo <i>University of Oulu</i>
Research Professor	Anssi Laukkanen <i>VTT Technical Research Centre of Finland</i>

Opponent

Professor	Pär Olsson <i>KTH Royal Institute of Technology</i>
-----------	--

Custos

Professor	Kai Nordlund <i>University of Helsinki, Department of Physics</i>
-----------	--

“Not all those who wander are lost”
– J.R.R. Tolkien

Printed version

ISBN 978-951-51-7766-7
ISSN 0356-0961

Unigrafia Oy
Helsinki 2021

Digital version

ISBN 978-951-51-7767-4

<http://ethesis.helsinki.fi/>

Electronic Publications @ University of Helsinki
Helsinki 2021

Author: Emil Levo
Title: **Radiation Damage in High Entropy Alloys**
Publisher: University of Helsinki, 2021, 72 p. + appendices, Report Series in Physics HU-P-D276
ISSN: 0356-0961
ISBN: 978-951-51-7766-7 (printed version)
ISBN: 978-951-51-7767-4 (digital version)

Emil Levo, **Radiation Damage in High Entropy Alloys**, University of Helsinki, 2021, 72 p. + appendices, Report Series in Physics HU-P-D276, ISSN 0356-0961, ISBN 978-951-51-7766-7 (printed), ISBN 978-951-51-7767-4 (digital)

Abstract

The development of future nuclear energy production concepts such as fusion and generation-IV fission reactors requires research in their respective component materials. Heavy radiation is commonplace in the proposed concepts, calling for durable, radiation tolerant materials that ensure long enough operational times for efficient energy production. The relatively new high entropy alloy materials, in which metallic alloys are built with several prevalent base elements, instead of just one base metal, have gained increased interest during recent years for their promise properties regarding various possible applications. Radiation tolerance is one promising property that high entropy alloys exhibit, meaning that they also have potential for use in nuclear reactors.

In this work we give a general introduction to radiation damage in nuclear reactors, the basic concept of high entropy alloys, computational means to study radiation damage in them, as well as research results from computational radiation damage studies of high entropy alloy like materials called equiatomic multicomponent alloys. The studies investigate radiation effects in various nickel-based equiatomic alloys, by classical molecular dynamic simulations. The main phenomena of interest are defect production, temperature effects and nanocrystalline structural stability of the alloys during irradiation in the form of massively overlapping cascade simulations.

In the studies it was found that the alloys exhibit a reduced defect ac-

cumulation with increased compositional complexity, that is to some extent upheld in a broad temperature range (138-800 K), and that the nanocrystalline structural stability is higher in the alloys than in pure nickel. The dislocation mobilities have been thought of as connected to the defect production. Here it is shown that dislocation mobility is reduced in the equiatomic alloys, similarly as in defect production, with an increase in compositional complexity. Additionally, the radiation damage production is validated by comparison with experiment, using a novel simulation method for Rutherford backscattering spectrometry in channeling conditions.

The general conclusion of this work is that, the high entropy alloy concept is promising in terms of the potential it shows for various future applications, such as nuclear reactors. Further studies are required, encouraged and supported by the results of this work.

Contents

Abstract	i
Contents	iii
Acknowledgements	v
1 Introduction	1
2 Purpose and structure	3
2.1 Summaries of the original publications	4
2.2 Author's contributions	5
2.3 Other publications	5
3 Radiation damage in metals	7
3.1 Regarding nuclear energy	7
3.1.1 Fission	9
3.1.2 Fusion	10
3.2 Damage by nuclear collisions	11
3.3 Materials durability	13
4 Metal alloys	19
4.1 Conventional alloys	19
4.2 High entropy alloys	21
4.3 Microstructure and nanocrystallinity	27
5 Methods	29
5.1 Molecular dynamics for radiation simulations	29
5.1.1 Classical molecular dynamics	29
5.1.2 Massively overlapping cascade simulations . .	34
5.2 Interatomic potentials	35
5.2.1 The embedded atom method potential	35
5.3 Radiation damage analysis	36
5.4 Rutherford backscattering in channeling conditions .	39
5.5 Simulation cell generation	39

6 Irradiation simulations of nickel-based equiatomic multicomponent alloys	43
6.1 Defect production	44
6.2 Rutherford backscattering in channeling conditions simulations	50
6.3 Temperature effects	52
6.4 Dislocation mobility	54
6.5 Nanocrystallinity	56
7 Summary and outlook	59
List of Abbreviations	61
List of Elements and Compounds	63
References	65
Publication I	73
Publication II	85
Publication III	99

Acknowledgements

I thank the Dean of the Faculty of Science Prof. Kai Nordlund, the Head of the Division of Materials Physics Prof. Flyura Djurabekova, the Head of the Helsinki Accelerator Laboratory Prof. Filip Tuomisto, as well as the former Heads of the Department of Physics Prof. Hannu Koskinen and Prof. Jyrki Räisänen for providing the facilities to conduct the research presented in this dissertation. Financial support from The Doctoral Programme in Materials Research and Nanosciences, Svenska Kulturfonden, Eurofusion and the Academy of Finland are gratefully acknowledged, as well as the computational time provided by CSC without which none of this would have been possible.

First I would like to thank my supervisor Dr. Fredric Granberg. Thank you Fredric, for all of the discussions, support and supplementary simulations for this project. You initiated this work back in your doctoral dissertation, and I am forever grateful for letting me be part of it.

I am very grateful for my supervising professors, Kai Nordlund and Flyura Djurabekova. I remember vividly and with great warmth my job interview for the summer student position that started all of this, in which my aptness for research was assessed by you. Thank you, for having such trust in me, little of which I had for myself too many a time, and for everything you taught me. Your knowledge and dedication in materials science is most impressive and truly inspiring – an ideal to strive for in the field.

I would like to thank all of my colleagues at the accelerator laboratory for a great working environment, insightful coffee breaks, and magnificent parties without which work would have been a lot more dull. A special thanks to Christoffer Fridlund and Annika Venäläinen, whom I miss immensely whenever I find myself needing a brief break from my current labour. Thank you Christoffer, for all of the help you gave me and others, in both school and work, and an even bigger thank you for introducing me to game jams. Thank you Annika, for all of the discussions and laughs, and your overly positive attitude which often helped me through my days.

Many thanks to all fellow students who have in some way shared my journey in studying physics. You made my time at the University of Helsinki and Lancaster University most worthwhile. Thank you Oliver Lybeck for an unforgettable year in Lancaster, and for a friendship I will always cherish. Not a day goes by in which I do not miss your antics. Thank you Isac Sahlberg, for helping me through my studies in theoretical physics. Your skill in mathematics still boggles me, and I miss those times you wrote equations on whatever surface you could find, trying to get me to understand.

A big, heartfelt, thank you to all my friends, who have been there for me, through the good times and the bad. Thank you to my closest group of friends from school, without whom life would have been a lot less memorable: Calle, Max, Viki, Ossi, Mara, Roope, Lassi, Tomma, Leo and Masa (the order is randomized). May there be plenty of memories to come. Thank you to Lauri Ketola, and to your whole family which I regard as my second one, for all of the support and love that you have given me throughout my life all the way from the beginning. You are, and will forever be, a brother to me.

Thank you to my family for the never ending well of support and patience they have had throughout this era of my life. I hope this book will shed some light on the mystical that has been my work for the past five years or so, for it would have never been written without your love. Finally I would like to thank Fanny for being there for me through the final push of finishing this work. Arguably, it was the most difficult part of the process, and would have been a lot more difficult without you.

Helsinki, December 3, 2021

Levo, Emil Nikolai

1 | Introduction

The usage of materials for different human purposes, whether those purposes be practical or otherwise, has been around for ages, and will be for ages to come. The first findings of gold in relation to humans date back to the Paleolithic period, while iron and nickel alloys were naturally found in meteors – therefore named meteoric iron – and was harvested by ancient Egyptians. One of the earliest written descriptions of composites as structural materials might be in the Old Testament where the Pharaoh forbids the supplying of straw for the making of brick (Exodus 5). Some hundred years before this, one of the oldest known customer complaints was written on a clay tablet, regarding a bad copper delivery [1].

Since those ancient days, the utilization of materials has grown and changed explosively, with new discoveries and trends sometimes becoming the very milestones in history with which we mark or describe whole eras: Going through the first tools in the stone age, the first purposeful alloying in the bronze age, the discovery of iron-working and early steels in the iron age, the impressive structures of classical antiquity, the first written works on metallurgy in the early modern era, up until the steel revolution of the industrial age, and the computer revolution in the silicon age.

The materials utilized by humans throughout the ages have ranged from organic to non-organic: wood, straw, cork and bone; metal, glass, plastic and stone. The study and further engineering of all the different materials – dead or alive – provided by our earth, falls under the behemoth umbrella of materials science. This behemoth employs a substantial amount of scientists, in the search for materials suited for current and future challenges of humankind, whether it be regarding something dramatic like an energy crisis and climate change, or something more mundane like better anti-stick heat-resistant frying pans. This work concerns itself with the more dramatic. Here, we take part in a fairly novel exploration of a new group of metallic alloys, called high entropy alloys, and their possible application in next generation nuclear reactors; although I would not mind a high

entropy alloy frying pan either. In terms of the behemoth umbrella, we now restrict ourselves to a smaller part of it, consisting only of metals and metallic alloys.

So if metals and their alloys have been part of human culture already during the time of the first known customer complaint, why is the exploration of these high entropy alloys such a novel thing then? Conventional metallic alloys are traditionally constructed to have one base metal with some attractive properties, and smaller additions of other elements to further tweak the properties to reach a desirable end result. The discovery of useful alloys constructed this way is reaching its limits, marking the end of a considerably long trend in metallurgy that started in the bronze age. High entropy alloys on the other hand have a different philosophy of synthesis. They do not have only one base metal, but consist of several metals at considerable proportions, and optional minor element additions. This philosophy in alloy construction leads to practically an infinite amount of possible high entropy alloys, in proportion to which only few have been studied, and even fewer actually synthesized, making our part of the behemoth umbrella even bigger.

Luckily we can further restrict ourselves in our exploration, by focusing mainly on the irradiation effects in high entropy alloys. Irradiation effects are important to study since nuclear reactors are ridden with radiation. These effects can be studied computationally as well as experimentally. The research done for this thesis is purely computational. However, there will be sections focusing on more general aspects of high entropy alloys, some experimental methods, and more in depth materials science for the more invested reader. All of the author's original results have been produced by molecular dynamics simulations, and compared to experiment where applicable, just to make sure we still are dealing with reality (to some extent at least). There is much to cover (even though we have restricted ourselves), and quite a lot to go through. So take a breath, and let us dive into one corner of the unexplored grounds of high entropy alloys, that lies under one of those proverbial umbrella monstrosities.

2 | Purpose and structure

The purpose of this thesis is to further the understanding of irradiation effects in high entropy alloys, in regards to their possible application in next generation nuclear reactors. Even though the term nuclear reactors is used in such a way that neither fission or fusion reactors are excluded, all of the work presented in this thesis has been conducted under the framework of building towards a future powered by fusion; one of humankind's greatest endeavours in finding a solution to the many energy production challenges we are faced with in today's world. Obviously we are not going to restrict the findings of this thesis only to building fusion reactors, rather, they should be applied wherever they can be of use. However, if you are a cookware manufacturer, and you do not intend to make your frying pan with the intent to be brought into an environment riddled with high energy irradiation, the results section might not interest you.

The publications included at the end of this article-based thesis, are presented and summarized briefly in this chapter, alongside with notes on the author's contributions to them. Chapter 3 presents the research problem by describing the radiation encountered in nuclear reactors, and the challenges that structural materials are expected to meet so that long operational times can be achieved to guarantee efficient energy production. Chapter 4 gives an overview of metallic alloys, and introduces the high entropy alloy family as well as the specific materials that are the subject of the studies in the articles. Chapter 5 describes the computational methods used for conducting and analyzing the irradiation simulations and chapter 6 presents the results of the simulations, compared with experiment wherever applicable. A summary and outlook of this work is given in chapter 7.

2.1 Summaries of the original publications

Publication I: Radiation damage buildup and dislocation evolution in nickel and equiatomic multicomponent nickel-based alloys

E. Levo, F. Granberg, C. Fridlund, K. Nordlund and F. Djurabekova
Journal of Nuclear Materials, **490** (2017), 323-332

We study the irradiation damage accumulated in four different nickel-based high entropy alloys during prolonged irradiation. The alloys were shown to have superior radiation resistance, in terms of a lesser defect accumulation during the irradiation, compared to pure nickel. A lesser defect mobility in the alloys, inherited from their disordered atomic structure, was seen to be a contributing factor. The results also reinforced previous findings, and showed that a smaller simulation cell is sufficient to obtain the damage trends, saving valuable computational time.

Publication II: Temperature effect on irradiation damage in equiatomic multi-component alloys

E. Levo, F. Granberg, K. Nordlund and F. Djurabekova *Computational Materials Science*, **197** (2021), 110571

We expand the 2017 study, by investigating the temperature effect on the irradiation damage accumulated in three different nickel-based high entropy alloys during prolonged irradiation. A novel computational Rutherford BackScattering in Channeling conditions (RBS/C) analysis was implemented, making direct comparison with experimental RBS/C spectra of irradiated samples possible. The study showed that the alloys exhibit a superior irradiation tolerance at temperatures ranging from 138 to 800 K. In addition, a substantial amount of defect data was produced with a possible use in simulations that need readily available defect data as input.

Publication III: Radiation stability of nanocrystalline single-phase multicomponent alloys

E. Levo, F. Granberg, D. Utt, K. Albe, K. Nordlund and F. Djurabekova
Journal of Materials Research, **34.5** (2019), 854-866

We look into the stability of nanocrystallinity in five different nickel-based high entropy alloys during prolonged irradiation at room temperature. The irradiation scheme was similar as in the studies described above, the only difference being in the structure of the simulation cells. In the previous studies the cells were single crystalline, while in this study nanocrystalline cells were created by Voronoi tessellation. The irradiation of these cells was continued until the nanocrystallinity diminished and the cells became practically single crystalline. The alloys showed to be more resilient to this transformation, and the initial orientation and geometry affected the transition time.

2.2 Author's contributions

In **Publication I** the author carried out the massively overlapping cascade simulations, analyzed most of the data, and wrote the publication.

In **Publication II** the author carried out the massively overlapping cascade simulations, ran the novel RBS/C calculations, analyzed most of the data, and wrote the publication.

In **Publication III** the author ran the massively overlapping cascade simulations, analyzed most of the data, and wrote the publication.

2.3 Other publications

Damage buildup and edge dislocation mobility in equiatomic multi-component alloys

F. Granberg, F. Djurabekova, E. Levo and K. Nordlund

Nuclear Instruments and Methods in Physics Research Section B: Beam Interactions with Materials and Atoms, **393** (2017), 114-117

3 | Radiation damage in metals

3.1 Regarding nuclear energy

To understand why we study novel materials such as high entropy alloys, and the irradiation response in them, it is worthwhile to look at what we are trying to build - nuclear reactors. Nuclear power is one of the largest sources of electricity in the world, after coal, hydro and natural gas. In 2018, about 12% of Europe's electricity was generated in nuclear fission power plants, while in tiny Finland the corresponding number was 35% [2]. Currently there are 443 nuclear power reactors in operation in the world, with 50 new reactors on the way [3].

Nuclear power is a topic that splits opinions, due to the many promises and threats that it brings with it. Arguments for nuclear power include: it being a low-carbon energy source, it has the lowest mortality rate compared to other energy sources, and it can reduce energy imports for countries. Arguments against nuclear power include: it increases the risk of nuclear proliferation, the problem of radioactive nuclear waste, expensive constructions, and the horrible accidents that poorly managed or constructed nuclear power plants can lead to such as in Chernobyl and Fukushima. All good arguments, but one has to remember that this debate focuses on nuclear fission power, and furthermore, on the current state of fission power.

The future of nuclear energy is full of promise. Generation IV fission reactors are being developed with the goal of generating sustainable energy with a minimal amount of nuclear waste, being extremely safe and reliable, being cost efficient and a reasonable option to other energy production concepts, and to be resistant to nuclear proliferation [4]. For reference, the Olkiluoto 3 fission reactor, that is being constructed in Eurajoki, Finland, is a generation III concept. In addition to development of nuclear fission power concepts, nuclear fusion power research has reached an important milestone in 2020, with the commenced machine assembly for the International Thermonuclear Experimental Reactor (ITER) in southern France. ITER

has the main goal of proving that fusion power is a feasible energy source, and aims to output 10 times more energy than what is put in. If proven feasible, the next step is the Demonstration Power Station (DEMO) that will upon completion be the first fusion device to be connected to the electrical grid. ITER and DEMO utilize so called Tokamak reactors that use magnetic confinement to achieve power through fusion reactions [5, 6], see figure 3.1.

One of the biggest challenges regarding the future of nuclear energy, is the question of what materials should be used in the structural components of a nuclear reactor [7, 8]. The components in nuclear reactors will be subject to various hazards, depending on the reactor type, such as corrosive environments, steep differences in temperature and magnetically controlled plasma [7, 9]. The one thing that will always be the unifying trait between different reactor types, is the irradiation. Regardless of whether we are talking about fusion or fission, next-gen or current-gen, or pressurized water reactor or molten salt reactor, components will always be subject to some amount of radiation. In the following, a brief explanation is given on the two types of nuclear reactions - fission and fusion - to provide a better understanding of, and context on, the origin of the materials irradiation problem in nuclear reactors.

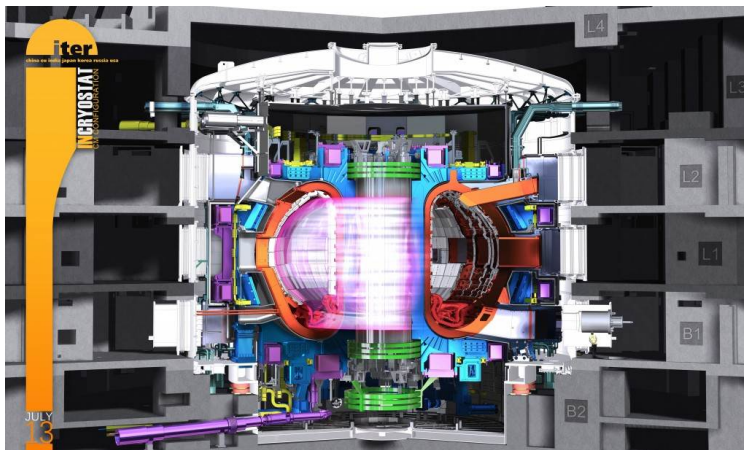


Figure 3.1: Schematic over the ITER fusion reactor (credit © ITER Organization, iter.org).

3.1.1 Fission

Fission is a nuclear decay process where an atomic nucleus splits into two lighter nuclei. It can be induced by bombarding heavy isotopes, such as uranium-235, with electrically neutral neutrons, resulting in an excited unstable uranium-236 isotope. Figure 3.2 depicts such an event, where the resulting uranium-236 fissions into krypton-92 and barium-141, as well as three new neutrons. The three new neutrons can also result in additional fission reactions, either in a controlled (nuclear fission powerplant) or an uncontrolled (nuclear bomb) manner.

The final isotopes and neutrons are so called fission products, and it is they that inherit the energy released in the fission reaction, in the form of kinetic energy. In a nuclear reactor, this kinetic energy, and some additional γ -rays, are then converted into heat, by collisions between the fission products and a so called working fluid (usually water). The heated working fluid will eventually turn a turbine, that produces electricity.

The highly energetic fission products and γ -rays will also interact with the rest of the reactor structure, which calls for radiation resistant materials that ensure long operational times of the power plant and structural integrity of the facility. The type of reaction seen in figure 3.2, lies at the heart of most nuclear plants connected to the electrical grid today, and should be associated with the controversial and highly debated nuclear power mentioned in the previous section.

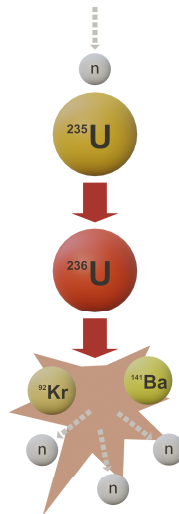


Figure 3.2: Nuclear fission reaction. A neutron (smaller grey sphere) is absorbed by an uranium-235 nucleus, turning it into uranium-236 for a moment. The excited uranium-236 isotope then splits into two lighter elements, and releases new free neutrons that can induce more fission reactions.

3.1.2 Fusion

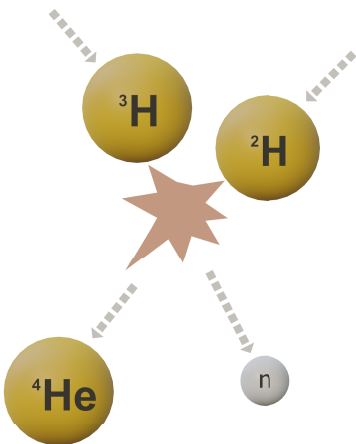


Figure 3.3: Nuclear fusion reaction. Deuterium (^2H) fuses together with tritium (^3H) to form helium-4, a neutron, and a whole lot of energy.

Fusion, one of the many holy grails of physics, can be thought of as the reverse to fission. In this case, instead of a heavy atomic nucleus falling apart, two light atomic nuclei fuse together. The protons and neutrons in atomic nuclei are bound together by the so called nuclear force. Two separate nuclei repel each other, due to the Coulomb force, and the fact that the nuclei are positively charged. To be able to bind together two nuclei, they need to be brought close enough, overcoming the Coulomb barrier, for a long enough time, so that the nuclear force will take over.

When that happens, the two nuclei form a new heavier nucleus, and a large amount of energy is emitted in the form of kinetic energy in the resulting new nucleus and additional neutrons or neutrinos, and possibly in γ -rays. An example of a fusion reaction can be seen in figure 3.3. Here, two isotopes of hydrogen, deuterium (^2H) and tritium (^3H), fuse together into helium-4, releasing a high energy neutron. In a fusion reactor, the highly energetic products of the fusion reaction will eventually interact with structural components, resulting in heat that will be transferred to a working fluid, that will turn the turbines to produce electricity. As in fission, the structural materials in fusion reactors need to be tolerant to radiation, in order to secure long operational times and structural integrity of the reactor. The reaction seen in figure 3.3 is the core event that future fusion reactors such as ITER builds upon, and might very well be a big part of the solution to humanity's energy problem.

3.2 Damage by nuclear collisions

At this point we can be safe in stating one thing: that there are high energy (> 1 MeV) neutrons involved in a nuclear reactor, be it powered by fission or fusion (note that we exclude any aneutronic concepts). Any high energy particles, such as ions, electrons, γ -rays and neutrons are able to modify material properties. The problem with neutrons, however, is that they have neutral charge, which makes them less likely to interact with atoms around them, so they can penetrate deep into the surrounding reactor materials. Eventually, the neutrons will interact with some nuclei, by scattering, being captured or inducing a fission event. The likelihoods of different neutron interactions with materials are represented by neutron cross sections, and are important when designing nuclear reactors so that neutrons can be used to our favour, while minimizing the damage they do to the rest of the materials in the reactor.

In a fission reactor for example, neutron cross sections are used as follows to achieve a controlled fission chain reaction (simplified): The fissile fuel has a high thermal neutron fission cross section so that it is likely to capture low energy neutrons (< 1 eV) and induce more fission events; The fuel is embedded in metal cladding with a low neutron absorption cross section, so that the neutrons are less likely to interact with the cladding; The fuel and the cladding (fuel cell) are surrounded by a moderator and working fluid with a high fast neutron scattering cross section to which most of the kinetic energy of the neutrons is transferred; Insertable control rods with high thermal neutron capture cross sections are used to control the chain reaction. But no matter how well a reactor is designed, stray neutrons eventually end up in the surrounding structural materials, resulting in radiation damage that can in the worst case lead to catastrophic failure [10, 11, 12] if not properly understood and prepared for.

It all starts on the atomic level. Materials like metals, and metallic alloys, usually have some simple crystal structure defined by a repetitive lattice. Two of the most common cubic crystal structures found in metals, Face Centered Cubic (FCC) and Body Centered Cubic (BCC), can be viewed in figure 3.4, where the spheres represent single atoms. When a high energy particle, such as a neutron, interacts with an atom in such a lattice by scattering, it gives away some of

its kinetic energy to the lattice atom. The lattice atom that was initially struck by the neutron, also called the Primary Knock-on Atom (PKA) or recoil atom, can be moved out of its lattice point if the transferred energy is large enough. Then the PKA goes on to further collide with other atoms in the lattice, that collide with more atoms in the lattice, resulting in a collision cascade, while the neutron has moved on to induce new localized collision cascades elsewhere.

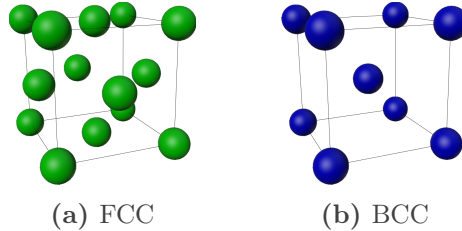


Figure 3.4: Basic cubic crystal structures.

A localized collision cascade, like in figure 3.5, typically results in a dense region called a heat spike, due to the very high kinetic energy the atoms have inherited from the neutron irradiation. The heat spike disappears after a brief while (order of picoseconds or 1×10^{-12} seconds), and most atoms return to lattice points. The atoms that do not, leave behind vacancies (empty atom sites) in the lattice. The displaced atoms are positioned in-between lattice points, and are called interstitials. Vacancies and interstitials are the most basic types of crystallographic defects found in metals, and are able to form larger more complex defect structures that eventually affect how material behaviour on a macroscopic level as well as their durability in nuclear applications. We will discuss different defect types in the next section (section 3.3).

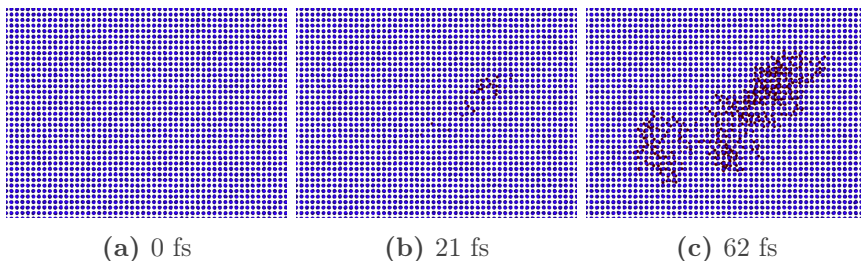


Figure 3.5: Collision cascade in FCC NiFeCr, by 15 keV recoil.

3.3 Materials durability

Several types of crystallographic defects can be created through irradiation processes in materials:

Zero-dimensional, point defects: interstitials, vacancies

One-dimensional, linear defects: dislocations

Two-dimensional, planar defects: surfaces, stacking faults

Three-dimensional, volume defects: defect clusters

Zero-dimensional point defects like the interstitial and vacancy, are the most basic type of defects, see figure 3.6. Empty lattice points are vacancies, while atoms inserted in between lattice points are interstitials. Corresponding interstitial-vacancies are known as Frenkel pairs. These are the primary defects created in collision cascades, as explained in the previous section.

One-dimensional linear defects, or dislocations, are irregularities in the arrangement of lattice atoms. Dislocations can, like point defects, be of vacancy or interstitial types. Common types of dislocations are the edge and screw dislocations. A simple edge dislocation can be seen in figure 3.7, where a layer of three atoms is missing in the distorted lattice on the right, when compared to the perfect lattice on the left. A screw dislocation on the other hand can be visualized by skewing the bottom left half of the atoms in the perfect lattice into the page, like a springboard from one end. Dislocations are most often represented by a so called Burgers vector. The Burgers vector for a given dislocation can be constructed by trying to accomplish a closed path in the distorted lattice around the dislocated area, as well as in the corresponding perfect lattice. The difference between the path in the distorted and perfect lattice represents the Burgers vector. Figure 3.7 visualizes this method, with the resulting Burgers vector in blue. For the screw dislocation the Burgers vector would point towards the reader.

Two-dimensional planar defects are quite abrupt irregularities in a crystallographic lattice that include surfaces and stacking faults. Surfaces are simply the end of the material, while a stacking fault is an irregularity in the periodicity of layers (or stacks) of atoms.

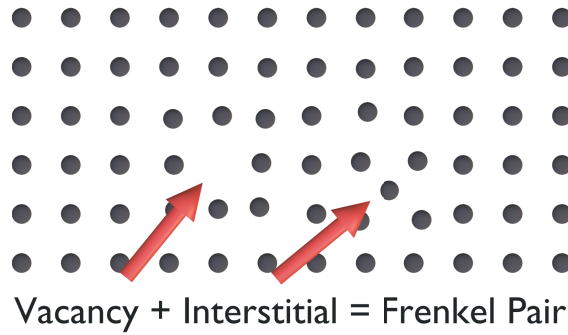


Figure 3.6: Point defects in two dimensional lattice.

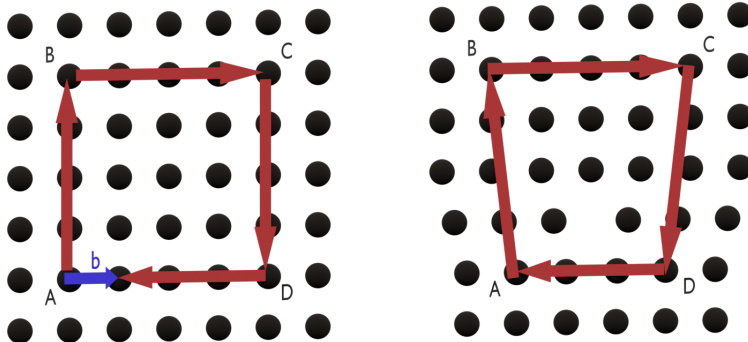
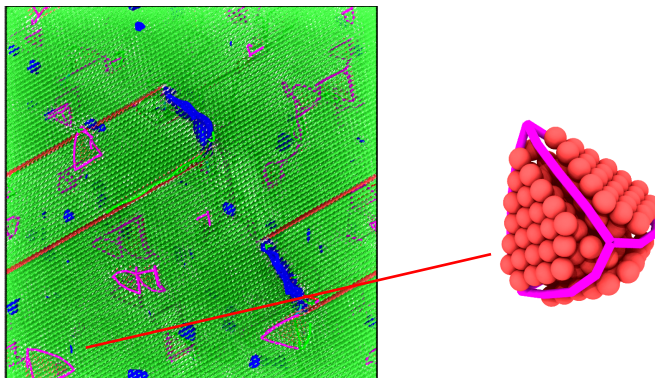


Figure 3.7: Edge dislocation with Burgers vector.



(a) Radiation damage in Ni. (b) Stacking fault tetrahedron.

Figure 3.8: Defects caused by prolonged irradiation in Ni.

Three-dimensional volume defects are more complex defect structures that can be formed as a result of the defects mentioned previously. Interstitials and vacancies can form large defect clusters, and dislocations can combine into large dislocation networks, see figure 3.8

Primary damage caused by irradiation events are the zero-dimensional point defects, as explained in section 3.2. Even though these defects are small, and invisible to the human eye, given enough time or external factors such as increased stress, temperature or more irradiation, the defects can through various processes migrate, combine, transform and grow, eventually affecting material properties on a macroscopic level. In a nuclear reactor this could mean property changes such as swelling and creep [13, 14], hardening, embrittlement [14, 15, 16], and in the worst case cracking.

By now, it should be evident that radiation in nuclear reactors needs to be properly understood, and the development of radiation resistant materials for nuclear applications is consequential for ensuring durable and safe operation of a nuclear power plant. The question now is, how do we actually understand radiation effects in materials? How do we measure it?

Several experimental methods exist for investigating irradiated material samples: *Rutherford BackScattering (RBS)* works by directing a beam of high energy ions onto a sample target, from which backscattered ions provide insight in the damaged microstructure of the material lattice [17, 18, 19]; *Transmission Electron Microscopy (TEM)* uses Bragg scattering of an electron beam to obtain information on defect types and positioning [20, 21, 22]; *Positron Annihilation Spectroscopy (PAS)* uses the lifetime and annihilation energy of implanted positrons to investigate vacancy type defects in materials [23, 24].

One challenge in measuring radiation damage is how it is related between different materials and differently irradiated materials. Displacements Per Atom (dpa) is one commonly used unit to measure primary damage in materials:

$$dpa = \frac{N_d(T_d)}{N} . \quad (3.1)$$

Here, N is the number of atoms in the studied system and N_d the

number of displaced atoms calculated with some model like the NRT-equation [25, 26, 27, 28, 29, 30, 31]:

$$N_d(T_d) = \begin{cases} 0, & T_d < E_d \\ 1, & E_d < T_d < 2E_d/0.8 \\ \frac{0.8T_d}{2E_d}, & 2E_d/0.8 < T_d < \infty \end{cases} . \quad (3.2)$$

Here, T_d is the damage energy that goes into the displacement of atoms, E_d is the Threshold Displacement Energy (TDE) that is required to create a Frenkel pair in the material lattice, i.e., the energy required to displace one atom. Equation 3.2 is a modification of the Kinchin and Pease model [25, 32] for atomic displacements. The modification was made by Norgett, Robinson and Torrens (hence the name) based on Binary Collision Approximation (BCA) simulations [26, 27] in which the possibility of ballistic processes recombining produced defects was taken into account [31].

Essentially, dpa tells us how many atoms have been displaced from their lattice site due to the primary radiation event. So, if a material is irradiated up to 1 dpa, this means in theory that every atom in the studied system has been displaced once. It is important to remember, that this unit does not in any way tell us how damaged a materials is. It simply is a measure of how many atoms are knocked around as the primary damage in the early stages of a recoil event (less than a picosecond). Recent work has made it clear that in metals it is actually not very accurate, as in heat spikes many more atoms are actually displaced than the NRT-dpa equation predicts [30]. Moreover, it tells us nothing of the retained damage in the long run (seconds to years), that is governed by the migration and recombination of defects, which depend on things like temperature and radiation dose rate.

Structural materials in nuclear reactors can reach more than 100 dpa during the operational lifetime. In Refs. 7 and 8, Zinkle et al. present five main radiation degradation threats in nuclear reactors: Radiation hardening and embrittlement, phase instabilities due to radiation induced precipitation, irradiation creep, swelling from void formation, and high temperature He embrittlement.

The complex machinery of current nuclear reactors require many different types of alloys to ensure stable and long lifetimes of power

plants. We want to go further with future concepts, such as generation-IV, and fusion reactors. This is where the need for new types of materials with suitable nuclear application properties comes in. In the next chapter, chapter 4, we will present one such novel material, a type of metallic alloy that differs from conventional alloys in its compositional philosophy: the high entropy alloy.

4 | Metal alloys

4.1 Conventional alloys

Ever since the dawn of metallurgy that lead to the Bronze Age of the human species, metallic alloys have been synthesized by adding metallic or non-metallic alloying elements to some prevalent base metal. Notable examples of metallic alloys, or simply alloys as we will call them hereafter, include bronze (base copper alloyed with tin) and steel (base iron alloyed with carbon), both of which have had a major impact on the formation of societies, cultures and the modern world as we know it. The main advantage with adding small concentrations of foreign elements to a base metal was early realised, as the ability to tweak material properties to ones own desires, that in ancient days mainly consisted of hardening and strengthening tools to improve their effectiveness and durability.

The motives now are the same as before, only the modern tools we want to improve include higher-tech inventions like nuclear reactors and spacecrafts. The necessity for differently tweaked alloys for specific applications is quite obvious in complex machinery such as nuclear power plants. For instance, consider the Pressurized Water Reactor (PWR) schematic in figure 4.1. It consists of a primary and secondary circuit, utilizing components such as the reactor core, coolant piping, and a generator; all of which need different types of alloys to meet their demands for successful operation [7].

In the schematic we can see several grades of steel, both stainless and not, denoted by different number combinations. Stainless steels are usually grouped in series, based on their crystal structure and elemental composition. For example the *300 Series* includes austenitic chromium-nickel steel alloys, and the *400 Series* includes ferritic and martensitic chromium steel alloys, both of which can be found in figure 4.1. The two latter digits in the number further separate the grouped steels, based on different elemental concentrations in the alloys, that results in different properties in the steels that are sought after in the various components of the power plant. For example

tweaking the concentration of chromium, or adding elements such as molybdenum will alter the steel's corrosion resistance, which is used in favour of some of the more corrosive environments in the reactor (some of these steels you can even find in your kitchen).

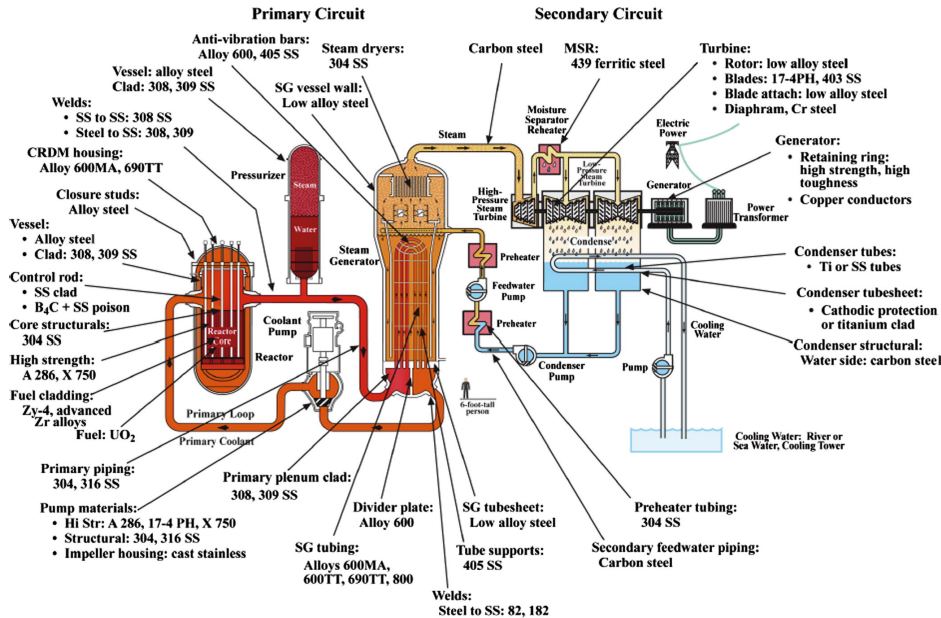


Figure 4.1: Schematic of a PWR with materials indicated where applicable¹.

We can also see more exotic alloys in the figure such as nickel-chromium superalloys (INCONEL) that are useful for high temperature and corrosion applications [33], and zirconium alloys (Zircaloy) that are usually used as the cladding for the nuclear fuel [7].

The complexity of nuclear reactors and the resulting need for a variety of materials with different application specific properties should be evident. Metallic alloys have proven to be a useful ally in the building of such reactors, but in terms of improving the properties of our currently utilized conventional alloys we might be running out of options. This is why a completely new philosophy of alloy design has taken root, and has rapidly gained increasing interest by scientists worldwide.

¹Reprinted from Ref. 7, with permission from Elsevier.

4.2 High entropy alloys

At the very beginning of the 21st century, two independent research teams, unknowing of each other, published their works on the development of alloys that differed from the conventional, in a not so unthinkable way: Instead of adding smaller fractions of alloying elements to some base metal, they designed their alloys with multiple base metals at equal proportions. In the paper published by Cantor et al., the alloys were called EquiAtomic MultiComponent (EAMC) alloys [34], while the paper published by Yeh et al. coined the term High Entropy Alloy (HEA) [35]. In Cantor's paper, focus lay on an FeCrMnNiCo alloy (an iron, chromium, manganese, nickel, cobalt alloy that is), while Yeh's paper presented a CuCoNiCrAl_xFe alloy (a copper, cobalt, nickel, chromium, iron alloy with a varying amount of aluminum). Both of these novel alloys had elements represented at equal proportions (except for the aluminum in Yeh's alloy), hence, the name EAMC alloy is quite fitting. But what did Yeh mean by high entropy?

Consider the combination of different types of atoms, in a simple crystal structure as in figure 4.2 with all positions of atoms randomized. The composition seen in figure 4.2 (a) could for example represent a steel with base iron and 2% carbon, while the composition in figure 4.2 (b) represents a five component HEA, like the one Cantor studied (FeCrMnNiCo).

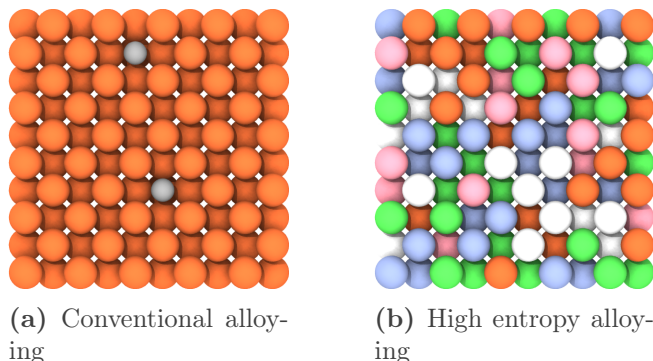


Figure 4.2: Visualization of different alloying principles. The differently coloured spheres represent different atom types.

The atoms in figure 4.2 are positioned according to the FCC crystal structure (go back to figure 3.4 for reference). We can see that the atoms are distributed randomly on the lattice of both alloys, making them something we call disordered solid solutions. Even though both alloys have disordered atomic mixtures, the degree of disorder is higher in the HEA. This disordered mixing can also be thought of as a measure of configurational entropy, which simply put, is the measure of the number of ways a system can be arranged. Configurational entropy of an alloy with different types of atoms, measures then all the possible arrangements of constituent atoms. The configurational entropy, for any theoretical alloy, can be obtained with equation 4.1:

$$\Delta S_{conf} = -R \sum_{i=1}^n c_i \ln c_i . \quad (4.1)$$

Here, ΔS_{conf} is the configurational entropy, R the ideal gas constant, n the number of elements in the alloy and c_i the proportion or weight of each element in the alloy. As it turns out, when you let the concentration c_i of each element be as close as possible to each other, the entropy ΔS_{conf} is maximized. Figure 4.3 shows a heatmap of the configurational entropy in a ternary alloy (alloy consisting of three elements). In it, we can see that the entropy is minimized in the three blue corners of the map, while it is maximized in the red centre. For a quaternary system (alloy with four elements) this figure would be of a tetragonal shape, with the entropy minimized in the corners, and maximized in the center region of the volume. The drawing and describing of the same graph for systems with more elements quickly becomes a headache, but luckily the concept stays the same with the entropy being minimized in the corner regions of the graph, while it is maximized in the middle, near-equiautomic, region.

Conventional alloys such as steels reside in the minimized blue corners of the heatmap, while the red central region is reserved for HEAs and the like. The red region is often referred to as something like “the vast unexplored centra of compositional phase space”. A mouthful for sure, but at the same time fascinating because of the fact of how unexplored it is, and the potential that region might hold in terms of technological development of the human species.

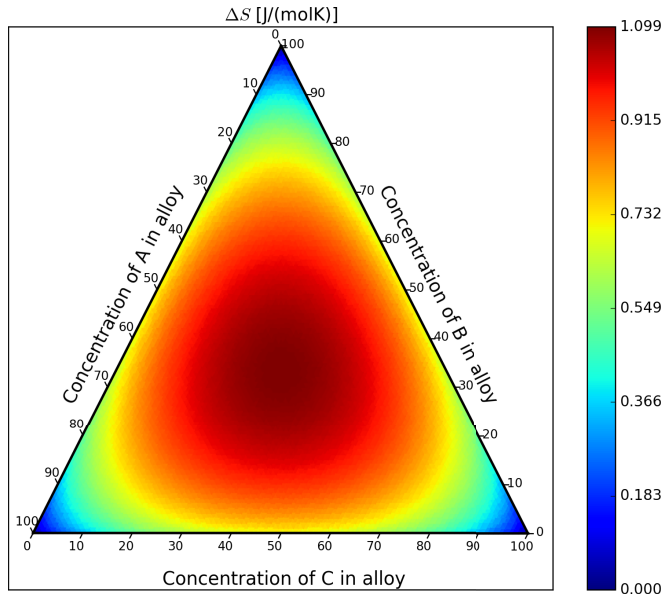


Figure 4.3: Configurational entropy for alloy with three elements [36].

As with any exploring, this brings with it also the tedious and confusing matters of naming things, setting borders and defining places. This is where we enter the jungle of names and definitions of alloys that are built in a multiprincipal manner, some of which are presented in the following.

High entropy alloy (HEA):

The most commonly used definition for HEAs is the one Yeh et al. proposed in their original 2004 paper [35]. According to it, an alloy with at least five different main elements, where each main element is represented between 5% and 35%, and possible minor element additions (<5%) can be regarded as a HEA. The number of elements in a HEA does not have an upper bound, but is for practical reasons often limited to 13 [35, 37]. Alternatively, we can think in terms of equation 4.1 as in reference 37 where it is stated that alloys with $\Delta S_{conf} > 1.5R$ are HEAs. This has further introduced the concepts “medium entropy alloys” ($1.5R \leq \Delta S_{conf} \leq R$) and “low entropy alloys” ($\Delta S_{conf} < R$) that include conventional alloys, like steel located in the periphery of composition space [37, 38].

MultiPrincipal Element Alloy (MPEA):

Often used as a synonym for HEAs, but works as a more ambiguous term that can also include alloys with less than five elements as long as they do not have only one base metal.

Equiatomic multicomponent alloy (EAMC):

Any alloy with all elements represented at exactly equal proportions. All EAMC alloys with at least five elements are HEAs according to the definition by Yeh et al. [35]. They are often talked about as a subgroup of HEAs, due to them being multiprincipal alloys at their maximized configurational entropy state. Publications I-III study EAMC alloys.

Single-Phase Concentrated Solid solution Alloy (SP-CSA):

Alloys with notable proportions of more than one element, and a microstructure consisting mainly of one phase (e.g. FCC) where solute atoms occupy lattice positions in the solvent lattice. More on microstructure and solid solutions in section 4.3. Due to a simple solid solution microstructure often formed in HEAs, they are talked about as a material group belonging to the SP-CSA family, but an SP-CSA does not necessarily have to be a HEA.

So, whenever you find yourself in a discussion about alloys with multiple main components, you might stumble upon one of the terms above. They tend to be used interchangeably, and this work serves to prove that point very well, given that the title mentions HEAs, while the papers presented at the end consider EAMC alloys. This is not a problem in our case, but does sometimes result in confusion, which is why it is good to have gone through the most common definitions of multiprincipally built alloys, and keep in mind that we wander on fairly unexplored grounds.

This novel philosophy in alloy design, of blending multiple principal elements, has led to studies that have uncovered and reviewed attributes including good mechanical properties [39, 40], wear resistance [39, 41], structural stability [39, 42], promising high-temperature behaviour [39, 40], oxidation and corrosion resistance [39], and high radiation tolerance [18, 19, 43, 44, 45, 46] in HEA like materials. For this thesis we are mostly interested in the radiation tolerance, which has shown itself as, for example, a reduced defect buildup [18, 19, 46] and resistance to volume swelling [43, 44].

Many of the promising properties and the tendency to form solid solutions in HEAs is usually attributed to four observed core effects [35, 37, 39]:

The high entropy effect is where HEAs get their name from, as explained previously. It is this higher configurational entropy that is theorized to contribute to the higher occurrence of simple solid solution phases in HEAs, instead of the formation of intermetallic and segregated phases that might be more brittle. This is achieved by the higher configurational entropy lowering the so called mixing free energy of a HEA system; an effect that is pronounced at higher temperatures.

The severe lattice distortion effect means that due to the differing sizes of constituent atom types in HEAs, the lattice of the resulting microstructure is distorted to a noticeable degree, see figure 4.4. This raises the free energy of a HEA like system due to the heightened strain of the lattice, and affects material properties by slowing down dislocation movement and further increasing solid solution strengthening, as well as lowering electrical and thermal conductivity. The lowered dislocation mobility will be important for us in chapter 6.

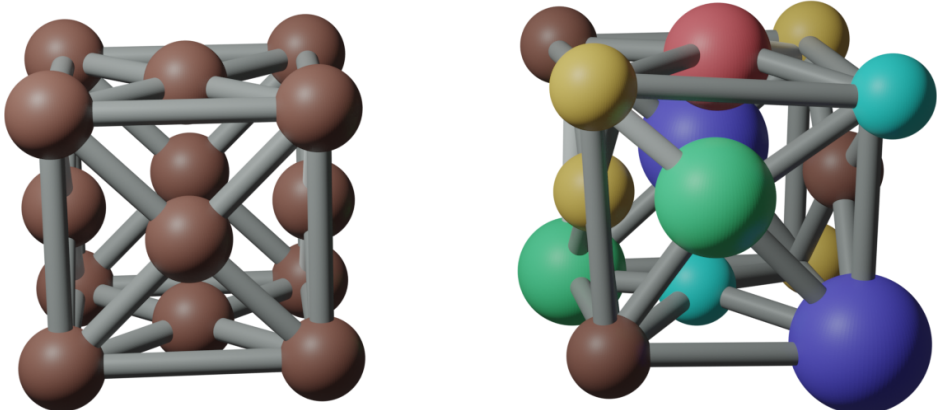


Figure 4.4: Comparison between a perfect single element (left) and distorted multicomponent (right) FCC unit cell.

The sluggish diffusion effect is the slow movement of atoms in HEAs, due to variations in local binding energies in the highly disordered and distorted alloy lattices. It has been hypothesized that this effect leads to the formation of nanocrystals in some as-cast HEAs, which in turn makes them promising as diffusion barrier coatings, and for the use in high temperature applications [35, 39]. However, this effect has also been disputed, due to the observation of slow diffusion being a secondary one, and because the observed diffusion might not even be any slower than in conventional alloys [47], which calls for more studies on the subject.

The cocktail effect simply means, as with any cocktail, that the different synergies between different constituent ingredients in a HEA can lead to significant, if not even unexpected, changes in material properties. As an example, the increase of aluminum, which is a soft metal, in the $\text{Al}_x\text{CoCrCuFeNi}$ system results in an increased hardness of the alloy [39].

Publications I-III present studies on various nickel based EAMC alloys. The term “nickel based” in this case has nothing to do with nickel being the most prevalent metal in the alloy, as in conventional alloys, rather, it means that the EAMC alloys that are studied all have nickel in common. The list of elements used in the studied EAMC alloys includes nickel (Ni), cobalt (Co), chromium (Cr), iron (Fe) and copper (Cu), forming the following alloys for each publication:

Publication I: NiCo, NiFe, NiCoCr, NiCoFe

Publication II: NiFe, NiCoCr

Publication III: NiCo, NiCoCu, NiCoFeCu

The computational methods used for studying radiation damage in the aforementioned EAMC alloys are going to be presented in the next chapter, chapter 5, but before that, a short word on the microstructure of HEA type materials.

4.3 Microstructure and nanocrystallinity

HEA like, multiprincipally built alloys, probably met a lot of skepticism in the early days of development (prior to the groundbreaking 2004 publications), due to them being expected to inherit a brittle, complex microstructure that would be of little use to anyone. The contrary happened, when both Yeh et al. and Cantor et al. showed in their respective publications that their five-element alloys both exhibited Simple Disordered Phase (SDP) FCC and BCC solid solution phases (see the simple crystal lattices in figure 3.4 for reference). A simple solid solution simply means that atoms of different elements share the same simple crystal lattice, such as FCC or BCC. The formation of solid solutions is particularly nice because of the strengthening that the alloy experiences, due to more difficult plastic deformation caused by strain fields that obstruct dislocation mobility.

Even though SDPs are commonplace for HEAs, this is not always the case, and different more complex phases have also been reported [39]. To ensure solid solution phases in binary systems, so called Hume-Rothery rules have been used in materials science [37]. These rules state requirements on the difference in atomic sizes, the crystal structure, the valency, and the electronegativity of the constituent elements. For HEAs however, the specific phase formation depends mainly on the enthalpy of mixing ΔH_{mix} , configurational entropy ΔS_{conf} (or entropy of mixing as it is also named in literature), and atomic size difference between constituent elements δ [37, 39].

Most often metals and alloys are not single crystalline, that is, they do not have one single crystal structure in one orientation that reaches out to the surface of the material. Rather, they are polycrystalline which means they consist of several crystallites, or grains, of some crystal structure, with different orientations in relation to each other, that are separated by grain boundaries. The sizes of the grains can vary from several millimeters, all the way down to the nanometer scale. When the grain sizes in a polycrystalline material are less than 100 nm, it is typically known as nanocrystalline. Figure 4.5 shows a nanocrystalline Ni cell. The green spheres indicate atoms that belong to an FCC lattice, while all other spheres can be seen as amorphous (missing a crystal structure). The green, FCC, areas are oriented differently and separated from each other by the amorphous

border, forming separate grains in the material. For this specific system, each grain had a radius of about 5 nm.

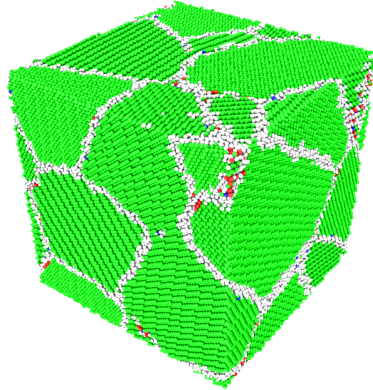


Figure 4.5: Nanocrystalline single phase (FCC) Ni cell with about 17 nm side length, and grain radii of about 5 nm.

The advantage of decreasing grain size comes from so called grain boundary, or Hall-Petch, strengthening, which has also been observed in HEAs [48]. When the grain sizes become smaller, the contribution of amorphous grain boundary volume becomes bigger. The amorphous grain boundaries impede dislocation motion, consequently strengthening the whole material. Equation 4.2 shows the so called “Hall-Petch” equation that relates the yield strength of a material with the size of the grains in it:

$$\sigma_y = \sigma_0 + \frac{K}{\sqrt{d}} . \quad (4.2)$$

Here, σ_y stands for the yield strength of the material, σ_0 and K are material specific constants, and d is the average diameter of the grains.

5 | Methods

Now the reader should have received a subtle introduction to nuclear energy, radiation damage, materials science, and HEAs. In this chapter we will focus on the computational physics part, and see how it can be used to study phenomena regarding all of the above. This is where things become a bit more technical, and we will primarily discuss how we implement everything we have gone through up till now mathematically for a computer to understand and conduct calculations on. Hopefully this will not discourage any reader who has made it thus far, as I will attempt to explain everything briefly and understandably for sufficient surface knowledge on each matter.

5.1 Molecular dynamics for radiation simulations

5.1.1 Classical molecular dynamics

Molecular Dynamics (MD) is a computational method with which one can simulate the movement and interactions between particles, such as molecules and atoms, in a selected system [49]. It is extensively used in materials science, biophysics and chemistry, and it is the main method of study used to produce most results presented in publications I-III.

MD takes a set of particles with pre-determined conditions, such as positions, velocities and possible constraints, to define the system one wants to simulate. The simulation is then carried out by updating all necessary particle information, for a given step forward in time, by solving numerically for Newtonian equations of motion, with the help of a so called interatomic potential that describes all interactions between the particles in the system. This updating of the system is then iteratively repeated for as long as necessary, until some final conditions have been met. For an irradiation simulation this might mean until the simulation sample that has been hit by a neutron, and became heated as a consequence, returns to its original temperature.

During the simulation, information such as the positions, energy and temperature can be output to gain valuable information on the sys-

tem's time evolution. For example, figure 3.5 visualizes an irradiation event simulated with MD, giving insight into how a collision cascade propagates in the material, and once it has propagated one can study the retained damage in the sample. Putting it quite simply, MD irradiation simulations can be viewed as a game of pool in three dimensions where the PKA is the cue ball.

Putting it less simply, please consider the flowchart in figure 5.1 that presents the basic steps of an MD cycle. This algorithm is a so called predictor-corrector algorithm, that solves numerically the atomic trajectories in the simulation. In the initial step, all simulated atoms are given positions \mathbf{r} and velocities \mathbf{v} , that are variable throughout the simulation. Then once the simulation starts, at the beginning of each iteration new positions and velocities are predicted for all atoms in the system. This is usually done by Taylor expanding so that

$$\begin{aligned}\mathbf{r}^P(t + \delta t) &= \mathbf{r}(t) + \delta t \mathbf{v}(t) + \frac{1}{2} \delta t^2 \mathbf{a}(t) + \frac{1}{6} \delta t^3 \mathbf{b}(t) + \dots \\ \mathbf{v}^P(t + \delta t) &= \mathbf{v}(t) + \delta t \mathbf{a}(t) + \frac{1}{2} \delta t^2 \mathbf{b}(t) + \dots \\ \mathbf{a}^P(t + \delta t) &= \mathbf{a}(t) + \delta t \mathbf{b}(t) + \dots \\ \mathbf{b}^P(t + \delta t) &= \mathbf{b}(t) + \dots\end{aligned}\tag{5.1}$$

where the P denotes the predicted value for the specified variable of an atom, \mathbf{a} is the acceleration and \mathbf{b} the time derivative of \mathbf{a} . The δt is the simulation time step that demonstrates how far forward in time the system progresses at the end of each iteration. More on the time step a little later.

The number of time derivatives of position that are used, define the order of the predictor-corrector algorithms. These are known as *Gear* algorithms [50], so that if only the terms presented in equation 5.1 are taken into account, it would be called Gear3. The simulation code PARallel CAScade molecular dynamics simulation code (PAR-CAS) [51, 52] that has been used for all simulations presented in this work utilizes the Gear5 algorithm, meaning that two additional time derivatives of position are added to equation 5.1.

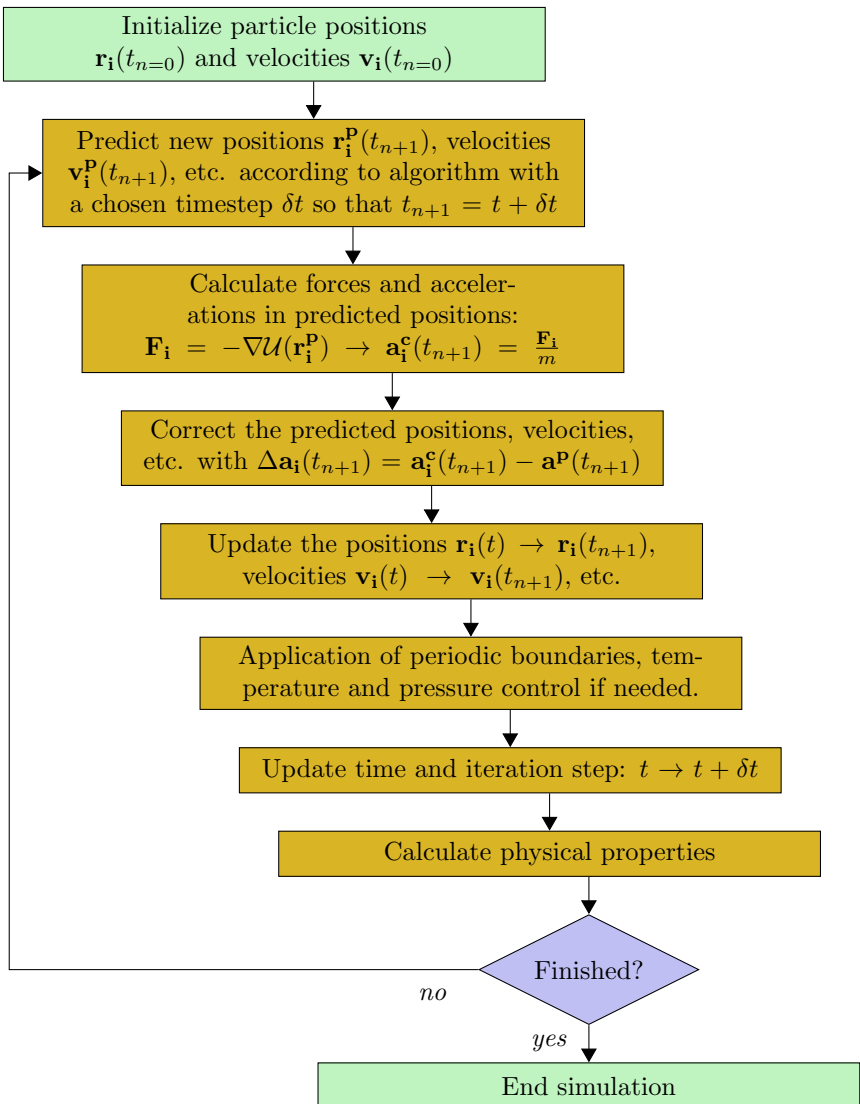


Figure 5.1: Molecular dynamics algorithm flowchart.

After the prediction step, a correction step is conducted. In the correction step, the correct accelerations are calculated in the predicted positions \mathbf{r}^P , with the help of an interatomic potential \mathcal{U} so that

$$\mathbf{a}^c(t + \delta t) = \frac{-\nabla \mathcal{U}(\mathbf{r}^P(t + \delta t))}{m}. \quad (5.2)$$

Here, the c denotes the correct value of the acceleration and m is the mass of the atom in question. The error of the predicted acceleration is then

$$\Delta \mathbf{a}(t + \delta t) = \mathbf{a}^c(t + \delta t) - \mathbf{a}^P(t + \delta t) \quad (5.3)$$

from which all predicted variables are corrected as

$$\begin{aligned} \mathbf{r}(t + \delta t) &= \mathbf{r}^P(t + \delta t) + c_0 \Delta \mathbf{a}(t + \delta t) \\ \mathbf{v}(t + \delta t) &= \mathbf{v}^P(t + \delta t) + c_1 \Delta \mathbf{a}(t + \delta t) \\ \mathbf{a}(t + \delta t) &= \mathbf{a}^P(t + \delta t) + c_2 \Delta \mathbf{a}(t + \delta t) \\ \mathbf{b}(t + \delta t) &= \mathbf{b}^P(t + \delta t) + c_3 \Delta \mathbf{a}(t + \delta t) \end{aligned} \quad (5.4)$$

where the coefficients c_i depend on the algorithm (c_2 is normally set as 1). Once the new variables have been predicted and corrected, some of them are scaled further depending on simulation constraints such as periodic boundaries, temperature- and pressure control.

Applying periodic boundaries means that if an atom reaches beyond the simulation cell boundary, it is simply returned into the cell on the opposite side. Periodic boundaries can be used in all three dimensions of the simulation cell, or only some of them, creating surrounding images of itself in desired directions. This repetition of the cell in all directions creates an infinite grid of the simulated material, modelling it in its bulk.

A Berendsen thermostat and barostat [53] are commonly used to control the temperature and pressure of the system if needed. For example, in our irradiation simulations the temperature needs to be controlled due to the collision cascade heating up the simulation cell.

In practice this is achieved by scaling atom velocities and positions with

$$\begin{aligned}\lambda &= \sqrt{1 + \frac{\delta t}{\tau_T} \left(\frac{T_0}{T} - 1 \right)} \\ \mu &= \sqrt[3]{1 - \frac{\delta t}{\tau_P} (P_0 - P)}\end{aligned}\tag{5.5}$$

for temperature and pressure control, respectively. Here, T_0 and P_0 are the temperature and pressure at time t , τ_T and τ_P are time constants with which the temperature and pressure are scaled, and T and P are the desired values for temperature and pressure.

Then, when everything is done, the iteration step can be updated and the system jumps forward in time with the time step. All physical properties that one can obtain, and are essential, should be output and stored. The time step for any MD simulation needs to be carefully chosen, so that energy is conserved in the calculations, and no atom overlap occurs. In irradiation simulations the time step is especially important, due to the high energy collisions in the system. This is why an adaptive time step is usually implemented for efficiency [54], like in PARCAS:

$$\delta t_{new} = \min \left(\frac{k_t}{v}, \frac{E_t}{Fv}, 1.1\delta t_{old} \right) .\tag{5.6}$$

Here, the new time step is evaluated by choosing the minimum value between the three terms inside the brackets. In the first two terms k_t and E_t are simply proportionality constants, while v is the velocity of the recoil and F is the total force experienced by the recoil. The final, term ensures that the new time step does not exceed the old time step by more than 10%.

This cycle is then repeated, as long as necessary, until all desired physical phenomena have been simulated. The output of such simulations should at least include the final atomic structure, possibly with individual atomic velocities and forces, as well as physical properties such as temperature, pressure and energy, so that an appropriate analysis of the simulation can be conducted.

5.1.2 Massively overlapping cascade simulations

All irradiation simulations studied in publications I-III follow a similar scheme to reach so called massively overlapping cascades in the studied materials. The term “massively overlapping cascades” signifies the repeated irradiation of the simulation cell, so that subsequent irradiation events enter a material with existing radiation damage. The simulation cell in our case has an FCC structure, with some hundreds of thousands of atoms, and periodic boundaries applied at all sides to mimic a material in its bulk.

A single irradiation simulation is initiated by giving an atom at the centre of the simulation cell an excessive amount of kinetic energy (the PKA). This atom will go on colliding with other atoms, initiating the collision cascade mentioned in 3.2, analogous to the cue ball in pool. The kinetic energy should be chosen with care, so that it will not melt the whole system. For our simulations, a 5 keV energy was used for the initial recoils, typical for a subcascade [18, 55]. High energy atoms lose energy to the surrounding electron configuration, which is why electronic stopping power was applied to account for this loss. During the simulation of a single collision cascade, Berendsen temperature control is applied at the border regions of the cell, to avoid excessive heating of the system. This is also why the PKA is chosen at the centre of the cell – to avoid the temperature controlled border region. Berendsen pressure control is applied as needed, in a separate relaxation simulation to eliminate any excess pressure buildup during the radiation.

This single irradiation simulation is then repeated, as necessary, in order to achieve massively overlapping cascades. In order to simulate homogeneous irradiation throughout the material sample, the cell is shifted by random magnitudes in all three dimensions without breaking the initial microstructure of it, due to the periodic boundaries. This ensures that the center region in which the recoil is initiated is effectively not the same throughout the whole irradiation simulation series. In publications I-III, the single irradiation simulations were typically repeated some thousand times, to reach a dpa around 0.3.

5.2 Interatomic potentials

To be able to evaluate the correct accelerations of the simulated atoms, and hence, the correct trajectories of the atoms, one needs a sufficient interatomic potential \mathcal{U} to describe atomic interactions for equation 5.2. For MD, an interatomic potential is usually constructed, so that its parameters are fitted to values describing physical properties obtained by either experiments or density functional theory calculations [56, 57]. This makes it so, that an interatomic potential is fit for use for some specific applications, but not for all. E.g., one potential might be good for simulating metallics, while another is better for an ideal gas.

Generally, a potential can be written as a series of many-body interactions:

$$\mathcal{U} = \sum_i^N \mathcal{U}_1(\mathbf{r}_i) + \sum_{i,j}^N \mathcal{U}_2(\mathbf{r}_i, \mathbf{r}_j) + \sum_{i,j,k}^N \mathcal{U}_3(\mathbf{r}_i, \mathbf{r}_j, \mathbf{r}_k) + \dots \quad (5.7)$$

Here, the first term corresponds with some external potential that all individual atoms are exposed to (for example an electric field), and is usually set to zero. The rest of the terms depend on relative positions for all atoms in regards to all other atoms, e.g. the second and third term describe two- and three-body interactions.

5.2.1 The embedded atom method potential

Embedded Atom Method (EAM) like potentials are most suitable for describing metallic systems [56, 58]. The method assumes each individual atom to be embedded in a sea of electrons, the density of which depends on the surrounding atomic environment. The total potential can be written as

$$\mathcal{U} = \sum_i^N F_i \left(\sum_j \rho(r_{ij}) \right) + \frac{1}{2} \sum_{i,j}^N \phi(r_{ij}) \quad (5.8)$$

where $\sum \rho$ is the electron density experienced by atom i , r_{ij} is the distance between atom i and j , and ϕ is a pair interaction function

(second term in equation 5.7). The pair interaction functions are normally divided into three parts for irradiation simulations:

$$\phi(r) = \begin{cases} \phi_{\text{ZBL}}, & r < r_1 \\ \phi_{\text{join}}, & r_1 \leq r \leq r_2 \\ \phi_{\text{fit}}, & r > r_2 \end{cases} . \quad (5.9)$$

Here, ϕ_{ZBL} is the Ziegler-Biersack-Littmark (ZBL) screened Coulomb potential [59] that answers for short range interactions and ϕ_{join} is a smooth joining function that connects the first part with ϕ_{fit} . The distances r_1 and r_2 are simply cutoff ranges that separate the three parts. The joining of the ZBL part with the rest of the potential is particularly important for irradiation simulations, due to it operating in the threshold energy region for defect production [60]. The EAM potential is fitted by constructing the functions F , ρ , and ϕ_{fit} .

To simulate the massively overlapping cascades in the nickel-based EAMC alloys and pure nickel for publications I-III, four different EAM type potentials were used to describe atomic interactions: The Zhou et al. [61], Lin et al. [62], Bonny et al. [63] and Purja Pun et al. [64] potentials. Different interatomic potentials for the same materials are known to possibly yield different defect behaviour in radiation simulations [65, 66], as will also be apparent in this work. This begs for the development of improved interatomic potentials for radiation simulations. Machine learning potentials, such as gaussian approximation potentials, have shown much promise lately due to a higher accuracy than provided by conventional potentials [67, 68]. However, machine learning potentials are currently computationally much slower than conventional ones.

5.3 Radiation damage analysis

In this work when we talk about radiation damage, we mainly consider crystallographic defects that are discussed in section 3.3. After an irradiation simulation, like each individual cascade simulation in our case, the final atomic structure should be stored for analysis of any retained damage. The atomic structure is needed since it is in its essence our irradiated material sample. In practice, the atomic

structure is stored in a text file where each row represents an atom, and holds information on the atom type, position, and velocity. This information can then be used by various methods that look into how each atom relates to the perfect crystal structure, which in our case is always FCC. In publications I-III the defect analysis laid most heavily on point defects (Frenkel pairs), defect clusters, different dislocation structures and the overall crystalline structure of the samples. In the following, the methods of defect analysis will be presented. It is good to point out separately here, due to its extreme usefulness in the computational materials science field, that the Open VIsualization TOol (OVITO) [69] was used extensively both to visualize the simulation cells (most of the simulation cell snapshots are taken with this tool), as well as to analyze them with the various modifiers included in it.

The Wigner-Seitz (WS) method is used to study point defects [51, 70]. The WS method divides the simulation cells into so called WS cells, that are a type of primitive cell in a crystallographic lattice, in which the WS cell contains exactly one lattice point. Each primitive cell can then be looked into, and the number of atoms in each cell tells us if it holds any interstitials, a vacancy, or a just single atom at its corresponding lattice point. In addition to obtaining the amount of point defects, their positions can also be found, as well as the element type in the case of interstitial defects.

OVITOs cluster analysis modifier is used, with the information obtained by the WS method, to study both interstitial- and vacancy-type defect clusters. The cluster analysis modifier uses a distance-based neighbouring criterion in order to determine whether defects belong to the same cluster or not (it can also use a topology-based approach). For our materials that have an FCC crystal structure, the cutoff for both interstitial and vacancy type defect clusters was chosen to be the distance between a lattice point and the midway point between its second and third nearest neighbours.

OVITOs Dislocation eXtraction Algorithm (DXA) modifier is used to determine different types of dislocations [71]. DXA works by dividing the atomic structure into good (nearly perfect lattice) and bad (defected lattice) crystal regions, that are separated by an interface mesh over which a Burgers circuit is swept to find and identify

dislocations. Once found, the dislocation line is drawn at the centre of mass of the circuit, examples of which can be seen in figure 5.2. The types of dislocations found in an FCC sample can be seen in the table on the left, with corresponding Burgers vectors and default colours in OVITO.

OVITOs Common Neighbor Analysis (CNA) modifier is used to classify the crystalline structure that sample atoms belong to [72, 73, 74]. The modifier offers four different operational modes, of which the adaptive CNA was used for this work. CNA evaluates what crystalline lattice an atom belongs to by looking at its neighbouring atoms. Three different values are calculated, regarding the different bonds between the investigated atom and its neighbours, and are compared to reference values in order to determine the crystal lattice the atom belongs to. Conventional CNA requires an input cutoff distance to be provided, while adaptive CNA removes this requirement. OVITOs representation of the different crystal structures can be seen in figure 5.2. The differently coloured atoms on the right belong to different crystal structures determined by the adaptive CNA method, and are clarified in the table on the left.

Structure	
Colour	Name
Green	Face-centered cubic (FCC)
Red	Hexagonal close-packed (HCP)
Blue	Body-centered cubic (BCC)
Yellow	Icosahedral coordination (ICO)
Dark white	Unknown structure (Other)

Dislocations (FCC reference)		
Colour	Burgers vector	Name
Dark blue	$1/2 < 110 >$	Perfect
Green	$1/6 < 112 >$	Shockley
Purple	$1/6 < 110 >$	Stair-rod
Yellow	$1/3 < 001 >$	Hirth
Light blue	$1/3 < 111 >$	Frank
Red	-	Other

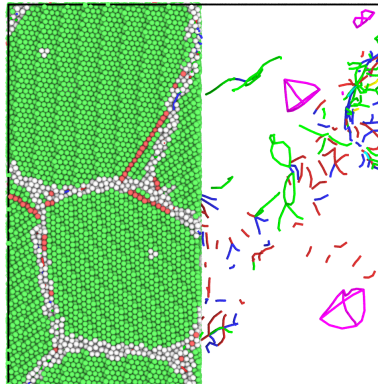


Figure 5.2: Table of crystal structures and dislocation types obtainable by OVITO, with an example snapshot produced with the CNA (left) and DXA (right) modifiers.

5.4 Rutherford backscattering in channeling conditions

One problem with the atomistic resolution in simulated radiation damage, acquired with the methods presented in 5.3, is how we relate it to reality. How can we be sure that the materials we irradiate by computation, compare well with their real life counterparts? One way of reassurance, is to simulate experimental analysis methods, and compare those with experimental analyses. One common method for experimentally analyzing real irradiated material samples for radiation damage, is the so called RBS/C method. This is why the RBS/C of Arbitrary Defected Crystals (RBSADEC) algorithm [75, 76, 77] was employed, to show that our simulations can be appropriately compared with experiment if need be.

RBS is, as stated back in section 3.3, an ion beam analysis method in which a beam of high energy ions are directed onto a material target sample, from which ions backscatter due to nuclear collisions with the target atoms. RBS/C uses this nuclear backscattering, to discover any obstructions in channeling directions of crystalline materials, such as the one seen in figure 5.3 (b). With a higher amount of obstructions in channels, a higher amount of backscattered ions are registered. Interstitial point defects might easily be assumed as the primary form of defects to be detected by the RBS/C method. However, it was observed in reference 75 that the RBSADEC signal was more sensitive to extended defects than point defects. Once the backscattering spectra of an irradiated sample has been calculated, it can be compared with pristine and completely destroyed samples, in order to determine the relative damage.

5.5 Simulation cell generation

The atomic structures, or simulation cells, used in the simulations conducted for publications I-III, are all stored in the *xyz*-format. This means that the number of atoms, dimensions of the simulation cell, and information on each atom is stored in a text file (the name *xyz* comes from the atomic coordinates that are stored in the file for each atom). The generation of the initial atomic structures is presented in this section, for all respective simulations.

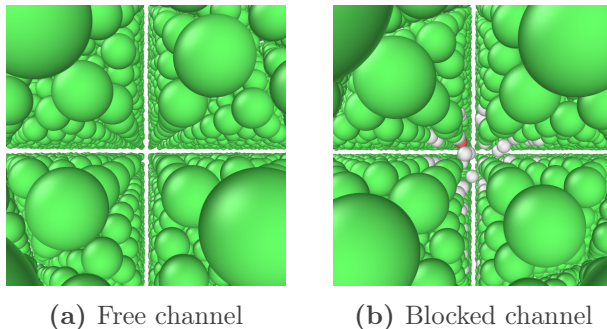


Figure 5.3: Free (a) and blocked (b) 100 channels in FCC nickel.

For publications I and II single crystalline cubic simulation cells were generated with an FCC crystal structure, to be used in the massively overlapping cascade simulations. In publication I, two different cell sizes were used. One had 108 000 atoms, and the other 500 000 atoms. 256 000 atom cells were used in publication II. Initial equilibrium simulations were performed, so that the 108 000, 256 000 and 500 000 atom cells obtained side lengths of about 10, 14, and 18 nm, respectively, in all dimensions. In publication III, cubic, nanocrystalline cells were created for all materials. The nanocrystals were created by Voronoi tessellation [78, 79, 80], resulting in 10 grains per cell, with grain radii of about 5 nm. All grains had an underlying FCC structure, but were oriented randomly. Each nanocrystalline cell contained about 450 000 atoms, and after an initial relaxation, the cells obtained side lengths of about 17 nm.

The element positions were randomized for all alloy simulation cells, with corresponding elemental proportions, to achieve completely disordered materials. In addition to this, three sibling cells were created for each material, with all atomic positions randomized differently. The three initial sibling cells were used, for three different simulation series of each material.

For the dislocation loop mobility simulations in publication III, simulation cells were created with a [1 1 0], [1 1 2] and [1 1 1] orientation in the x -, y - and z -directions, respectively. The cells were elongated in the x -direction, in which the dislocation loops were supposed to move freely. The final size of the cells was approximately $(35 \times 13 \times 12)$ nm³. Two <110> interstitial dislocation loops with different radii (5 and

10 Å) were inserted in the cells.

For the RBS/C analysis in publication II, 62 irradiated cells (from the massively overlapping cascade simulation) were merged together according to a nuclear energy deposition depth profile, so that different depths corresponded with different doses of irradiation. These slabs were created for all of the materials and their corresponding simulation series. The final slabs analyzed by RBSADEC were about 900 nm long.

6 | Irradiation simulations of nickel-based equiatomic multicomponent alloys

In the following sections, the main results of publications I-III will be presented for various Ni-based EAMC alloys. First, we will consider the defect production at room temperature (300 K) in NiCo, NiFe, NiCoCr and NiCoFe (publications I-II). Second, we take a look at the simulated RBS/C spectra in NiFe and NiCoCr at room temperature, and compare them with experiment (publication II). Third, we consider the above at different temperatures (publication II). Fourth, we consider the dislocation mobility in NiFe and NiCoCr (publication I-II). Last, we look into the behaviour of nanocrystalline NiCo, NiCoCu and NiCoCuFe during massively overlapping cascades (publication III).

All studies utilize the classical MD code PARCAS to simulate massively overlapping cascades, in their respective material simulation cells. For all materials, three different simulation series were ran with randomized initial atomic structures (arrangement of elements in the alloys) and recoil directions. Most data obtained from these simulations are mean values from these three sibling simulations. In addition to running massively overlapping cascades, supportive dislocation mobility simulations and RBS/C calculations were conducted.

Even though several EAM type potentials were utilized to describe the atomic interactions in the different studies, mostly results using the Zhou et al. and Lin et al. potentials will be presented for brevity. For more in depth differences between the different potentials, please see the publications.

6.1 Defect production

The defect production in various Ni-based EAMC alloys has been extensively studied in publications I-II. All studies used the same method of massively overlapping cascades to model radiation damage in the simulation cells, but with different simulation cell sizes, and different materials. Publication I presents results for both a 500 000 and 108 000 atom simulation cell for the materials NiCo, NiFe, NiCoCr, NiCoFe and pure Ni for reference. The use of two different cell sizes was motivated by finding out whether the same trends in point defect evolutions could be observed for a larger (more accurate) and a smaller (computationally less expensive) simulation cell. Publication II compromises between these two cell sizes using a 256 000 atom simulation cell for the materials NiFe, NiCoCr and pure Ni for reference.

The point defect evolution of NiCo, NiFe, NiCoCr, NiCoFe and pure Ni from publication I can be seen for the smaller cell in figure 6.1 and for the larger cell in figure 6.2. For the smaller cell, we can not see an as clear trend in most defects to least defects, as for the larger cell, although we can clearly say that Ni and NiCo are in that regard above NiFe, NiCoCr and NiCoFe. The trend is much clearer for the larger cell. We can see that Ni has the most defects, then comes NiCo, NiFe and NiCoFe, and lastly NiCoCr with the least number of defects. This indicates a clear point defect accumulation reduction in EAMC alloys, as compared to the pure base element, with the addition of new alloy constituents. It is also clear that the choice of element affects this reduction when comparing NiFe with NiCo and NiCoCr with NiCoFe.

Also note that the point defect accumulation trend is reversed in the early dose regime. This is much clearer in figure 6.2 at about <0.05 dpa. Here we can see that Ni and NiCo are below the rest of the alloys. This was confirmed by running a multitude of single cascade simulations in the same materials, where a higher defect amount was observed in NiFe, NiCoCr and NiCoFe compared to Ni and NiCo. This is explained by a higher probability of vacancy formation in the former alloys, during the recrystallization phase of a heat spike [45].

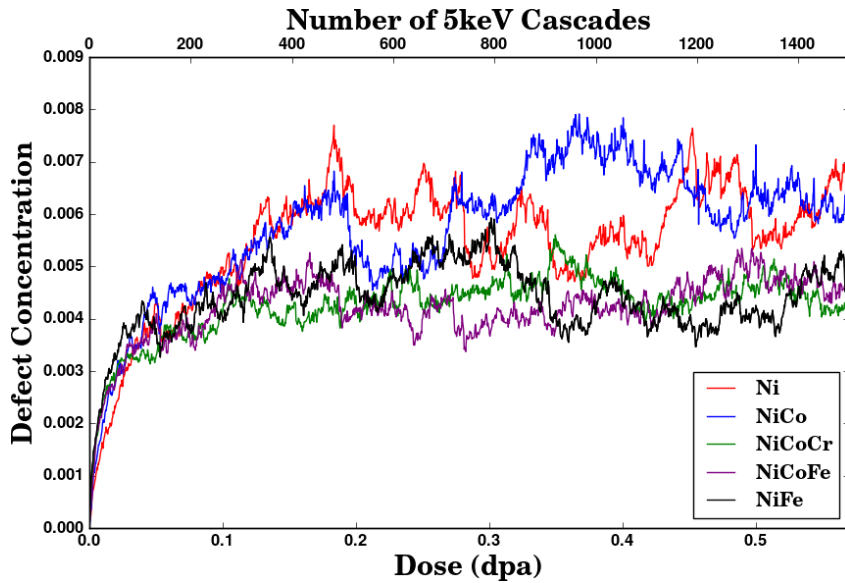


Figure 6.1: Point defect concentration evolution during prolonged irradiation in simulation cell with 108 000 atoms [81].

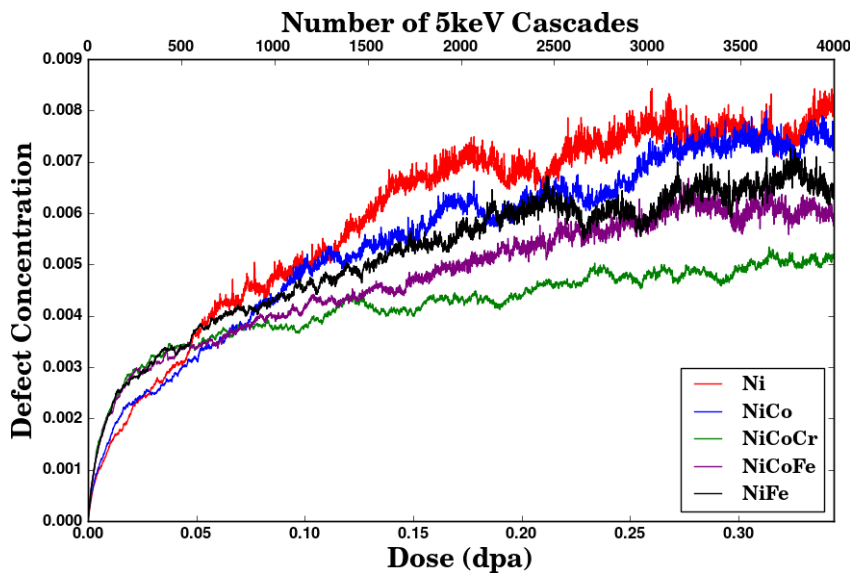


Figure 6.2: Point defect concentration evolution during prolonged irradiation in simulation cell with 500 000 atoms [81].

An indicative concentration of Stacking Fault Tetrahedra (SFT) was calculated for the large cells in publication I, and can be seen in figure 6.3. This number was obtained by taking the amount of stair-rod dislocations (see table in 5.2) in the simulation cells, and dividing that amount by six, due to there being six stair-rod dislocation lines in an SFT. In the figure we can see clearly two groups of materials. Ni and NiCo that exhibit a higher amount of SFTs, and NiFe, NiCoCr and NiCoFe that have a lower amount of SFTs.

Figure 6.4 shows snapshots of dislocation networks and defect clusters at a late stage in the simulations, after approximately reaching saturation of radiation damage. In the snapshots we can see the same thing qualitatively as in figure 6.3, that is, a higher amount of SFTs in Ni and NiCo, compared to NiFe, NiCoFe and NiCoCr. In addition to seeing SFTs and stair-rod dislocations in Ni and NiCo, large shockley-partial loops and frank loops are observed. In NiFe, NiCoFe and NiCoCr, there is a much more pronounced occurrence of small shockley-partial dislocation loops.

The similarities between Ni and NiCo is not that surprising, given that Ni and Co are that similar. They are next to each other in the periodical table, with similar masses, electronegativity and similar crystal structures at room temperature (FCC and Hexagonal Close Packed (HCP) respectively). The added complexities of Fe and Cr reduces both the point defect accumulation and the formation of SFTs, which drives the point of how HEA type alloys can be tolerant to radiation damage, given that enough elements of specific types are added into the mix.

In addition to explaining the differences in defect production with similarities and differences between elements, and the number of elements in specific EAMC alloys, the difference in defect production has also been acknowledged to different dislocation mobilities in the materials [18, 45]. It was visually observed that there seemed to be more mobile dislocation structures in the Ni and NiCo simulations, compared to the NiFe, NiCoFe and NiCoCr simulations. This is why supplemental dislocation mobility studies have been performed, which are presented in section 6.4.

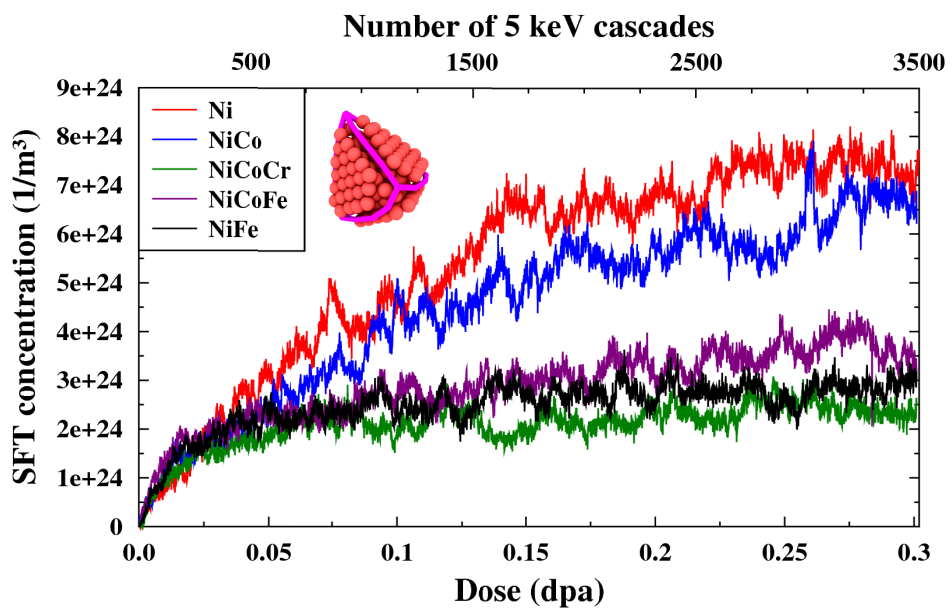


Figure 6.3: SFT concentration during prolonged irradiation [81].

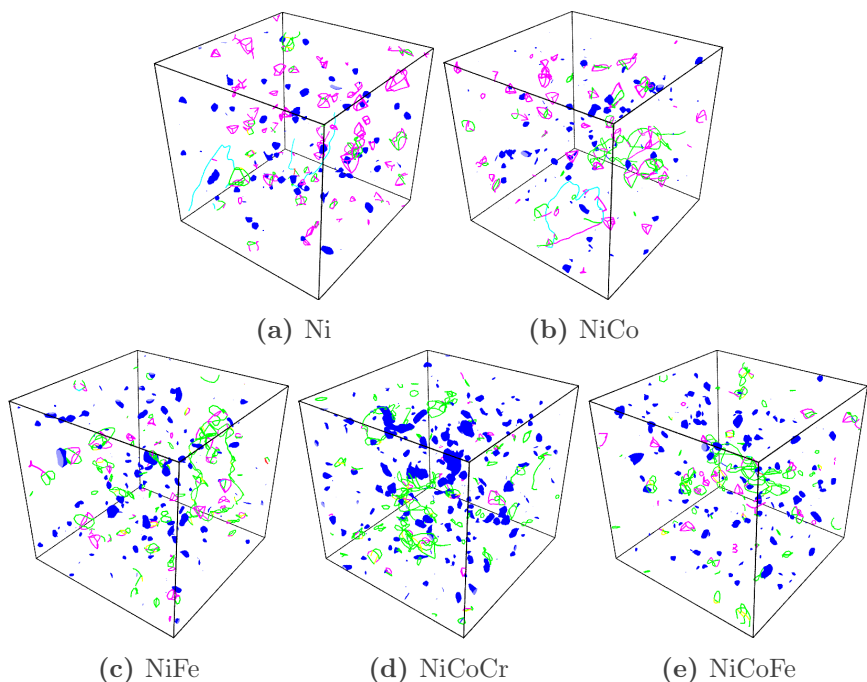


Figure 6.4: Dislocation networks after 0.3 dpa.

Defect clusters were studied in more detail in publication II for NiFe, NiCoCr and pure Ni. The evolution of the amount of differently sized defect clusters can be seen in figure 6.5 and 6.6 for interstitial and vacancy clusters, respectively. Each line in the plots represent a specific cluster size, specified by the legend. For the interstitial clusters we can see that Ni exhibits large clusters already at a relatively low dose, compared to NiFe and NiCoCr, while the vacancy clusters show an opposite phenomenon.

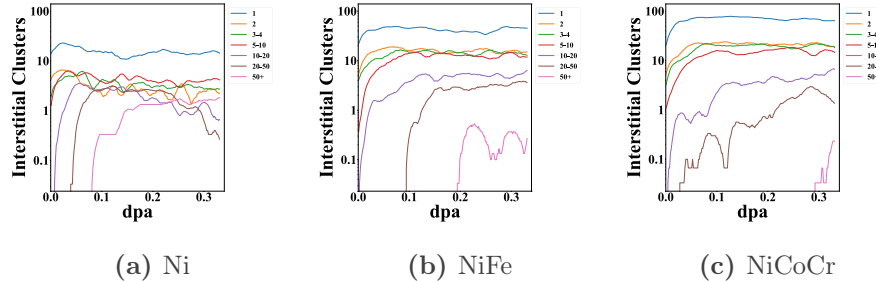


Figure 6.5: Number of differently sized interstitial clusters during prolonged irradiation [82].

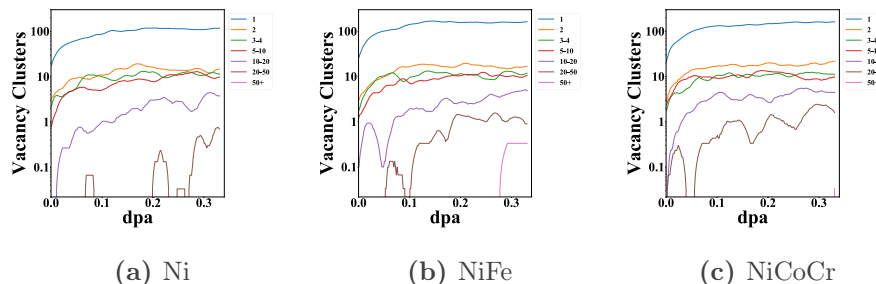


Figure 6.6: Number of differently sized vacancy clusters during prolonged irradiation [82].

In addition to looking at the defect cluster sizes, the interstitial clusters were studied in more depth by analyzing what elements they consisted of in NiFe and NiCoCr. Figure 6.7 and 6.8 shows the proportions of different elements in the interstitial clusters for NiFe and NiCoCr, respectively. For NiFe, we can see that Ni is more prevalent in the clusters than Fe, except for the very largest clusters where they are represented almost equally. Likewise for NiCoCr, we can see that Ni is the most occurring element, then comes Co, then Cr.

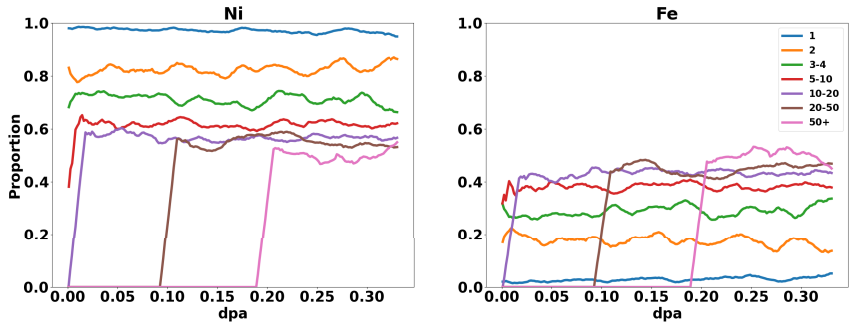


Figure 6.7: Element proportions in interstitial clusters for NiFe [82].

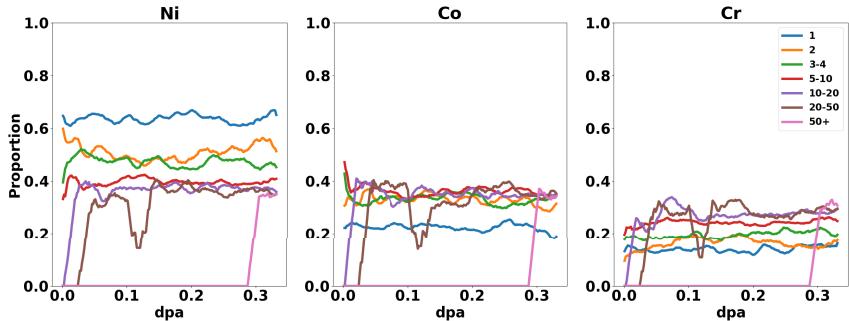


Figure 6.8: Element proportions in interstitial clusters for NiCoCr [82].

6.2 Rutherford backscattering in channeling conditions simulations

RBS/C simulations were utilized in publication II to be better able to compare our results with experiments. The RBSADEC code was used for this purpose, by running it on almost 900 nm long slabs, constructed by stacking cells together from the irradiation simulations. The individual cells were obtained from different doses corresponding to different depths in a material, according to a nuclear energy deposition profile. In addition to running RBS/C simulations on the irradiated cells, corresponding pristine materials slabs were also analyzed to obtain two reference profiles, one completely perfect, undamaged profile (ion beam directed in channel), and one completely destroyed profile (ion beam tilted from channel). Samples with spectra closer to the destroyed reference profile, are seen as samples with more radiation damage.

The obtained RBS/C spectra for NiFe, NiCoCr and reference Ni can be seen in figure 6.9. Note that here are included results obtained also from experiment [77], and calculations using the Bonny et al. potential. The experimental part is included to see how our irradiation simulations fare in terms of radiation damage picked up by the RBS/C method, when compared to experiment. The additional potential was included to see, which of the potentials produce more “realistic” spectra.

In the graph, we can see a similar trend as in the point defect evolution. The most damaged material is pure Ni, then comes NiFe, and last is NiCoCr. This trend is the same for both the Zhou et al. and Bonny et al. potentials, as well as the experimental spectra. However, the computed spectra do differ from the experimental ones. The Bonny et al. potential overestimates the damage for Ni drastically, while the Zhou et al. potential overestimates it only a little. For NiFe, Bonny et al. has almost a one to one similarity with experiment, while Zhou et al. overestimates just a little. For NiCoCr the Zhou et al. also overestimates the damage. The overall better agreement between the experimental spectra, and the computational one produced with the help of the Zhou et al. potential, is the reason why mainly the Zhou et al. results are shown in the previous, and the following sections.

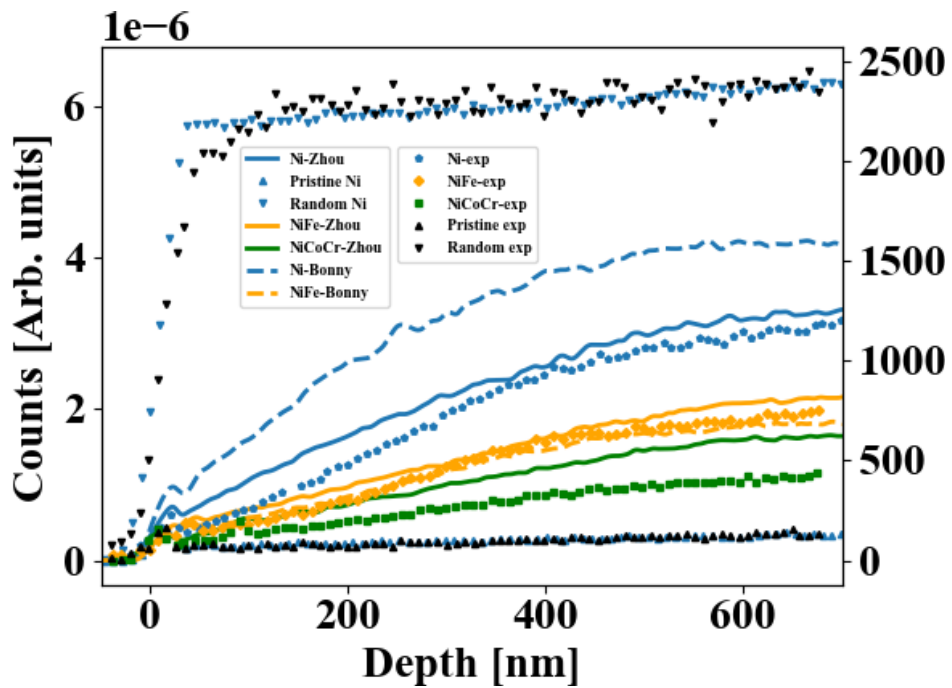


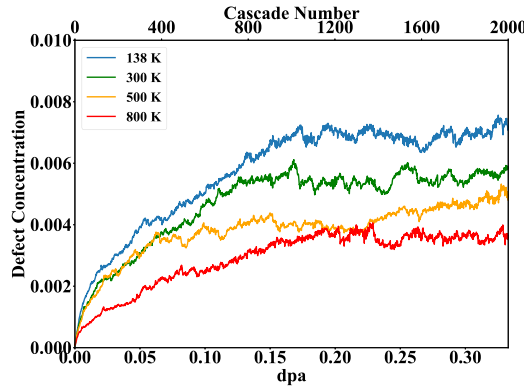
Figure 6.9: Comparison between simulated and experimental [77] RBS/C spectra [82].

6.3 Temperature effects

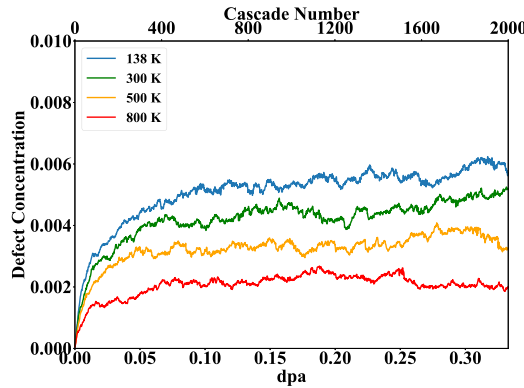
The large temperature differences occurrent in nuclear reactors requires the study of how massively overlapping cascades produce damage at different temperatures. Publication II mainly focuses on how temperature affects radiation damage in NiFe and NiCoCr, compared to pure Ni, by simulating massively overlapping cascades at 138, 300, 500 and 800 K. The simulation cells, consisting of 256 000 atoms were irradiated up to a dose of about 0.3 dpa. This publication also utilized an RBS/C analysis using the novel RBSADEC code, in addition to the conventional point defect analysis in publication I. Due to the multitude of data visualization for the temperature effect study, the reader is encouraged to view publication II for a full review. Here we present only graphs on the point defect accumulation at different temperatures, and describe the rest of the main findings in text.

Figure 6.10 shows the point defect concentration at the different temperatures, for each material separately. We can see that for all of the materials, there is at least a factor of two difference in the final saturated defect concentration when comparing the lowest and highest temperatures. The drastic lowering of point defects with the increase in temperature is especially interesting, due to the fact that the higher amount of recombination events that is expected when raising the temperature, is a long term effect that should not be observable at our simulated time scales.

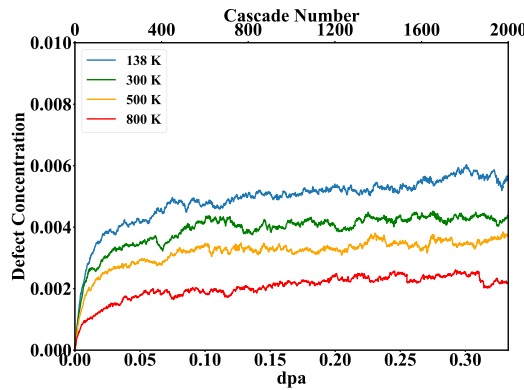
When comparing the materials to each other at the different temperatures, it was seen that NiFe and NiCoCr perform better than pure Ni, following the same trend as in publication I at all temperatures except 500 and 800 K. At the higher temperature the alloys did exhibit less point defects than Ni, but the alloys themselves were not distinguishable from each other in terms of which one performed better. In the RBS/C spectra, however, the ordering was the same at all other temperatures as at room temperatures, i.e. Ni performed worst, then came NiFe, and NiCoCr performed the best, in terms of least backscattered counts.



(a) Ni



(b) NiFe



(c) NiCoCr

Figure 6.10: Point defect evolution at different temperatures during prolonged irradiation [82].

6.4 Dislocation mobility

The reduced defect accumulation in EAMC alloys has been partly hypothesized to be a consequence of a lesser dislocation mobility. This is why both edge dislocation and dislocation loop mobility studies were performed in EAMC alloys for publication I and II.

The edge dislocation mobility simulations in reference 45 and publication I were performed with $\frac{1}{2}[1\ 1\ 0]$ edge dislocations in FCC simulation cells with the orientations [1 1 0], [1 1 2] and [1 1 1], in the x -, y - and z -directions, respectively, for Ni, NiCo, NiFe, NiCoFe and NiCoCr. Different onset stresses were applied to the system, and the resulting velocities of the dislocations measured. The results can be seen in figure 6.11. In the figure up until about 250 MPa we can see a clear ordering of highest mobility to lowest, as Ni, NiCo, NiFe/NiCoFe and NiCoCr, similarly as in the point defect evolution in figure 6.2.

Due to the more complex nature of dislocation loops and networks, as seen in the dislocation snapshots in figure 6.4, additional dislocation loop mobility simulations were also performed for publication II. Two differently sized perfect [1 1 0] interstitial loops were created in similar simulation cells as for the edge dislocation, but only for Ni, NiFe and NiCoCr. Once relaxed, the interstitial loop became a shockley-partial loop, similar to those seen in figure 6.4. No external force was applied to get the dislocation loops moving, so all movement was thermally activated. The loops were simulated at two temperatures, 300 and 600 K, for a total of 5 ns. The resulting movement in the x -direction of the cell can be seen in figure 6.12. From the figure, it is evident that practically no thermally activated movement can be observed at 300 and 600 K, for either loop size, in the EAMC alloys. In pure Ni however, the dislocation loop moves readily for both loop sizes, and temperatures.

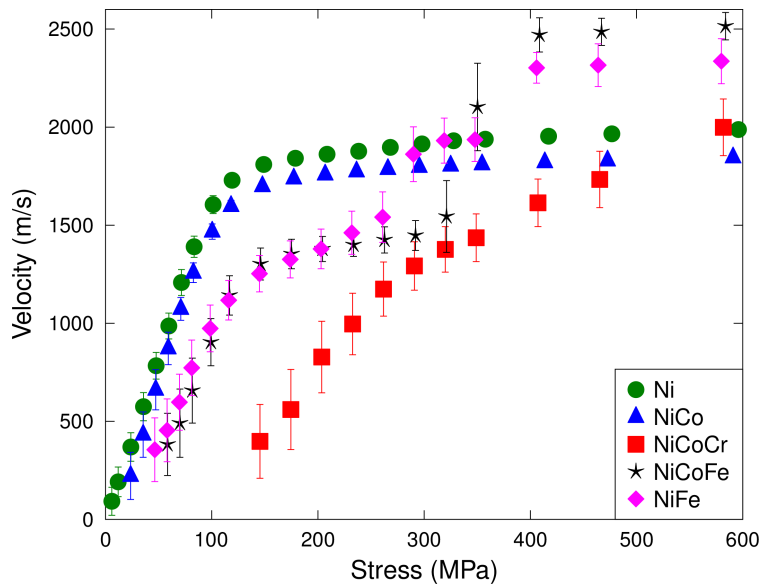


Figure 6.11: Stress induced edge dislocation mobility [81].

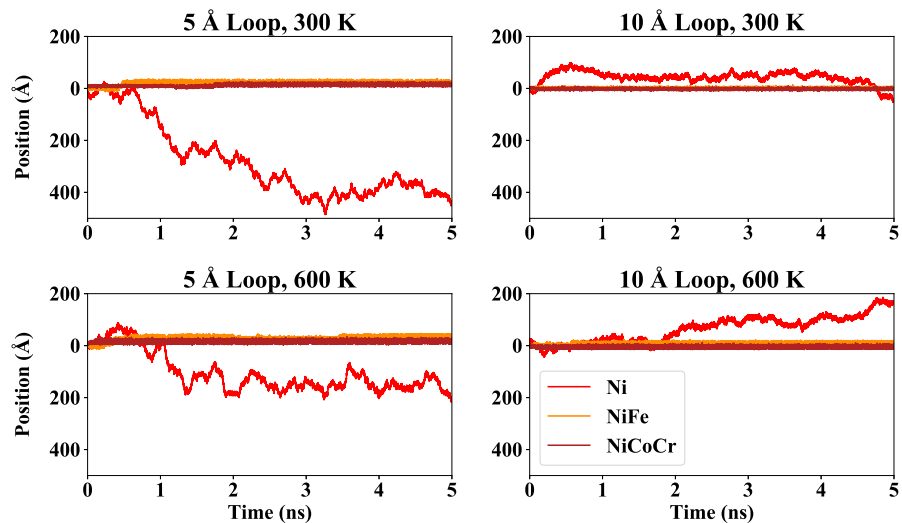


Figure 6.12: Thermally activated dislocation loop mobility [82].

6.5 Nanocrystallinity

All results on massively overlapping cascade simulations presented above, and in publications I and II, study simulation cells with a single crystalline structure. Since single crystals are not feasible for most applications, most materials are in some polycrystalline form anyway, and the added advantage from going even smaller by reducing grain sizes to the nanoscale, publication III studied massively overlapping cascades in nanocrystalline EAMC alloys.

For the simulations, three different initial nanocrystalline cells were created using Voronoi tessellation. Atoms of different elements were randomly distributed in these cells, as before, to form the EAMC alloys NiCo, NiFe, NiCoCu and NiCoFeCu. In addition to the EAMC alloys, we also created nanocrystalline Ni, Ni₃Fe and Ni₂Fe cells to simulate as references. The resulting cells had a little less than 500 000 atoms positioned into 10 grains with radii of approximately 5 nm and corresponding grain boundaries. In the actual irradiation simulations, it was quickly found that some of the materials did not retain a single phase FCC structure in the grains, but BCC phases became relevant. Depending on the potential, and the stability of the single phase grain structure, some of the unstable materials were excluded from this study (e.g. NiFe is missing from results presented here). One of the initial nanocrystalline cells can be viewed in figure 6.13 (a), and for a zoomed in version figure 4.5. These initial cells were irradiated using the massively overlapping cascade simulation scheme, until the nanocrystalline structure failed. The rest of figure 6.13 (b-e) shows the evolution of the nanocrystalline cell for Ni during said irradiation, and we can see how the grains merge together due to it.

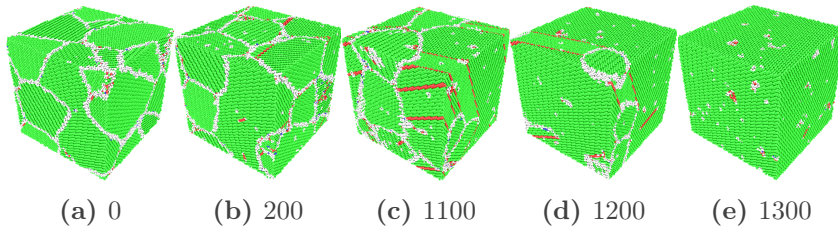


Figure 6.13: Evolution of nanocrystalline Ni during prolonged irradiation. Cascade number in subcaptions.

The main interest of the study was to see how many cascades it takes for the materials to transform into the single crystal like structure seen in figure 6.13 (e). The point of failure was defined as when the percentage of atoms belonging to an FCC lattice exceeds 90%. This point can be seen for some of the materials in figure 6.14. Note that, for every initial nanocrystalline structure, there is a different collapsing point denoted by different geometric shapes.

Not surprisingly, we see that pure Ni is the quickest to collapse for each of the initial nano-structures. The longest surviving nano-structure is found in the reference Ni_2Fe , but, at the same it exhibits one of the widest spreads between the different initial cells. Many more simulations would be needed in reality, to get a good mean value of the cascade number at which the transformation occurs, but this would be computationally very expensive (as these simulations already proved to be) making it unfeasible. Looking at the EAMC alloys, we can see that the best performing one is NiCoFeCu . Interestingly, we see that when adding an additional element to NiCo (Cu), we can see a lowering of the transformation point, while additional Fe is needed for improved performance, putting a stress yet again on the importance of element synergies.

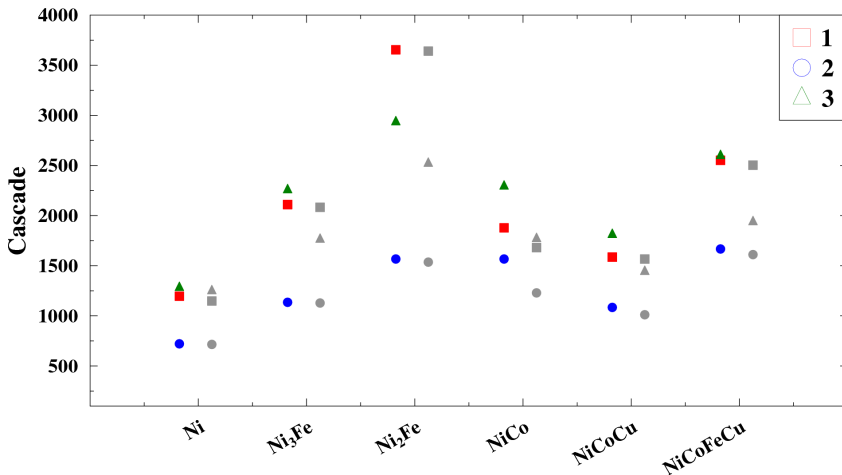


Figure 6.14: Number of cascades to achieve >90% FCC (coloured) and FCC+HCP (grey) in the different nanocrystalline cells (determined by shape) [83].

7 | Summary and outlook

In this dissertation we present an introduction to the novel HEA family, alongside with research results from three computational radiation damage studies, in the context of developing materials for next generation nuclear reactor technologies. More specifically, we have studied radiation damage in various Ni-based EAMC alloys, related to the HEA family, by computational means. The classical MD code PARCAS was used to simulate massively overlapping cascades in the materials, for publications I-III.

In publication I we studied the point defect concentration and dislocation network evolution, alongside with stress induced edge dislocation mobility, in Ni, NiCo, NiFe, NiCoFe and NiCoCr at room temperature. A reduced point defect accumulation was observed with an increased complexity in the EAMC alloy composition, supporting earlier findings [18]. An indicative number of SFTs was also seen to be reduced in the alloys. The edge dislocation mobility simulations showed a similar trend in the reduction of dislocation velocity, as in the defect study. The results also showed that a compromise in simulation cell size can be made, saving valuable computational time.

In publication II we studied how temperature affects the defect production, alongside with thermally activated dislocation loop mobility, in Ni, NiFe and NiCoCr. Here we saw that the same defect reduction is observed in the EAMC alloys, when compared to Ni, however, the difference in point defect concentration between NiFe and NiCoCr is less pronounced at higher than room temperatures. The dislocation loop mobility simulations showed thermally activated dislocation movement only in Ni, while the dislocations appeared stationary in the alloys. Additionally, the novel RBSADEC code was utilized to calculate RBS/C damage spectra for the irradiated materials, which proved to be an efficient way to compare the depth distribution of radiation damage between our simulations and experiment.

Publication III differed from the rest of the studies by investigating a nanocrystalline cell, instead of a single crystalline one. Here the main goal was to study the stability of the nanocrystalline structure

during the massively overlapping cascades, i.e., how many cascades did it take to merge all grains into an approximately single crystalline cell, in Ni, Ni₂Fe, Ni₃Fe, NiCo, NiFe, NiCoCu and NiCoCuFe. The study showed that all EAMC alloys had a more stable nanocrystalline structure than Ni. Initial grain structure showed to be of importance, due to the different doses at which the different sibling simulation cells transitioned into a single crystal.

The results found in publications I-III are promising, encouraging further studies of HEA type alloys and their potential use in future nuclear energy concepts. The exact nature of HEA applications in nuclear reactors are still being researched, and it is very likely that the final elemental compositions in nuclear HEA components are very different to the ones discovered by Cantor and Yeh et. al, and those studied for this work. For example, a lot of promise lies in BCC HEAs based on heavy elements such as tungsten (W). As stated before, there are practically an infinite amount of HEA like materials waiting to be studied for various applications in and outside of nuclear, meaning a lot more research in specific alloys is needed. Computational methods can be a useful tool for this purpose, as shown in this work, but this also calls for more research on interatomic potentials for MD to be able to describe the many-element interactions in these multiprincipal materials, and the radiation effects in them. Machine learning potentials might be one avenue for improvement in this regard.

This work is a small part of a much greater endeavour in propelling the human species into the next age of energy production, in which a looming energy crisis is ideally averted and the negative effects of climate change are hopefully minimized. On a personal note, even though it is yet unclear exactly in what applications HEA like materials are going to be found in the future, it would be surprising indeed if they are found nowhere. One should maybe not expect another industrial revolution induced by HEAs (like with the mass production of steel), but it would not be unthinkable to one day hear about high entropy coatings in nuclear reactors, or on kitchen utensils.

List of Abbreviations

- BCA** Binary Collision Approximation
- BCC** Body Centered Cubic
- CNA** Common Neighbor Analysis
- dpa** Displacements Per Atom
- DXA** Dislocation eXtraction Algorithm
- EAM** Embedded Atom Method
- EAMC** EquiAtomic MultiComponent
- FCC** Face Centered Cubic
- HCP** Hexagonal Close Packed
- HEA** High Entropy Alloy
- MD** Molecular Dynamics
- MPEA** MultiPrincipal Element Alloy
- OVITO** Open VIualization TOol
- PARCAS** PARallel CAScade molecular dynamics simulation code
- PAS** Positron Annihilation Spectroscopy
- PKA** Primary Knock-on Atom
- PWR** Pressurized Water Reactor
- RBS** Rutherford BackScattering
- RBS/C** Rutherford BackScattering in Channeling conditions
- RBSADEC** RBS/C of Arbitrary Defected Crystals
- SDP** Simple Disordered Phase
- SFT** Stacking Fault Tetrahedra
- SP-CSA** Single-Phase Concentrated Solid solution Alloy

TDE Threshold Displacement Energy

TEM Transmission Electron Microscopy

WS Wigner-Seitz

ZBL Ziegler-Biersack-Littmark

List of Elements and Compounds

C_o cobalt

C_r chromium

C_u Copper

F_e iron

N_i nickel

W Tungsten (wolfram)

References

- [1] A. L. Oppenheim. “Letters from Mesopotamia: official, business, and private letters on clay tablets from 2 millenia” (1967).
- [2] *International Energy Agency*. <https://www.iea.org/>. Accessed: 2021-03-16.
- [3] *International Atomic Energy Agency*. <https://pris.iaea.org/pris/>. Accessed: 2021-03-16.
- [4] OECD Nuclear Energy Agency. *Technology Roadmap Update for Generation IV Nuclear Energy Systems*. 2014.
- [5] V. P. Smirnov. “Tokamak foundation in USSR/Russia 1950–1990”. *Nuclear fusion* 50.1 (2009).
- [6] G. G. Dolgov-Saveliev, D. P. Ivanov, V. S. Mukhovatov, K. A. Razumova, V. S. Strelkov, M. N. Shepelyev, and N. A. Yavlin-sky. “Investigations of the stability and heating of plasmas in toroidal chambers”. *Proceedings of the 2nd Geneva Conference on the Peaceful Uses of Atomic Energy*, p. P/2527. 1958.
- [7] S. J. Zinkle and G. S. Was. “Materials challenges in nuclear energy”. *Acta Materialia* 61.3 (2013).
- [8] S. J. Zinkle and J. T. Busby. “Structural materials for fission & fusion energy”. *Materials Today* 12.11 (2009).
- [9] S.J. Zinkle, A. Möslang, T. Muroga, and H. Tanigawa. “Multimodal options for materials research to advance the basis for fusion energy in the ITER era”. *Nuclear Fusion* 53 (2013).
- [10] INES IAEA. “The international nuclear and radiological event scale”. *User’s Manual* (2008).
- [11] R. Wakeford. “The Windscale reactor accident—50 years on”. *Journal of Radiological Protection* 27.3 (2007).
- [12] International Atomic Energy Agency. *The Fukushima Daiichi Accident*. 2015.
- [13] L. K. Mansur. “Theory and experimental background on dimensional changes in irradiated alloys”. *Journal of Nuclear Materials* 216 (1994).
- [14] N. I. Budylkin, E. G. Mironova, V. M. Chernov, V. A. Kras-noselov, S. I. Porollo, and F. A. Garner. “Neutron-induced swelling and embrittlement of pure iron and pure nickel irradiated in the

- BN-350 and BOR-60 fast reactors”. *Journal of nuclear materials* 375.3 (2008).
- [15] B. A. Gurovich, E. A. Kuleshova, Y. A. Nikolaev, and Y. I. Shtrombakh. “Assessment of relative contributions from different mechanisms to radiation embrittlement of reactor pressure vessel steels”. *Journal of Nuclear Materials* 246.2-3 (1997).
 - [16] E. A. Kuleshova, B. A. Gurovich, Z. V. Bukina, A. S. Frolov, D. A. Maltsev, E. V. Krikun, D. A. Zhurko, and G. M. Zhuchkov. “Mechanisms of radiation embrittlement of VVER-1000 RPV steel at irradiation temperatures of (50–400)° C”. *Journal of Nuclear Materials* 490 (2017).
 - [17] L. C. Feldman, J. W. Mayer, and S. T. A. Picraux. *Materials analysis by ion channeling: submicron crystallography*. Academic Press, 2012.
 - [18] F. Granberg, K. Nordlund, Mohammad W. Ullah, K. Jin, C. Lu, H. Bei, L. M. Wang, F. Djurabekova, W. J. Weber, and Y. Zhang. “Mechanism of Radiation Damage Reduction in Equiatomic Multicomponent Single Phase Alloys”. *Physical Review Letters* 116.13 (2016).
 - [19] Y. Zhang, G. M. Stocks, K. Jin, C. Lu, H. Bei, B. C. Sales, L. Wang, L. K. Béland, R. E. Stoller, G. D. Samolyuk, et al. “Influence of chemical disorder on energy dissipation and defect evolution in concentrated solid solution alloys”. *Nature Communications* 6 (2015).
 - [20] R. F. Egerton et al. *Physical principles of electron microscopy*. Vol. 56. Springer, 2005.
 - [21] T. Matsui, S. Muto, and T. Tanabe. “TEM study on deuterium-irradiation-induced defects in tungsten and molybdenum”. *Journal of Nuclear Materials* 283 (2000).
 - [22] D. J. Edwards, E. P. Simonen, F. A. Garner, L. R. Greenwood, B. M. Oliver, and S. M. Bruemmer. “Influence of irradiation temperature and dose gradients on the microstructural evolution in neutron-irradiated 316SS”. *Journal of Nuclear Materials* 317.1 (2003).
 - [23] R. N. West. “Positron Studies of Lattice Defects in Metals”. *Positrons in Solids*. Springer Berlin Heidelberg, 1979, pp. 89–144.

- [24] S. Abhaya, R. Rajaraman, S. Kalavathi, and G. Amarendra. “Positron annihilation studies on FeCrCoNi high entropy alloy”. *Journal of Alloys and Compounds* 620 (2015).
- [25] G. H. Kinchin and R. S. Pease. “The displacement of atoms in solids by radiation”. *Reports on progress in physics* 18.1 (1955).
- [26] M. T. Robinson and I. M. Torrens. “Computer simulation of atomic-displacement cascades in solids in the binary-collision approximation”. *Physical Review B* 9.12 (1974).
- [27] M. J. Norgett, M. T. Robinson, and I. M. Torrens. “A proposed method of calculating displacement dose rates”. *Nuclear engineering and design* 33.1 (1975).
- [28] O. A. Waseem and H. J. Ryu. “Tungsten-Based Composites for Nuclear Fusion Applications”. *Nuclear Material Performance*. InTech, 2016.
- [29] K. Nordlund, S. J. Zinkle, A. E. Sand, F. Granberg, R. S. Averback, R. Stoller, T. Suzudo, L. Malerba, F. Banhart, W. J. Weber, et al. “Improving atomic displacement and replacement calculations with physically realistic damage models”. *Nature communications* 9.1 (2018).
- [30] K. Nordlund, S. J. Zinkle, A. E. Sand, F. Granberg, R. S. Averback, R. E. Stoller, T. Suzudo, L. Malerba, F. Banhart, W. J. Weber, F. Willaime, S. L. Dudarev, and D. Simeone. “Primary radiation damage: A review of current understanding and models”. *Journal of Nuclear Materials* 512 (2018).
- [31] K. Nordlund, S. J. Zinkle, T. Suzudo, R. S. Averback, A. Meianander, F. Granberg, L. Malerba, R. Stoller, F. Banhart, B. Weber, F. Willaime, S. Dudarev, and D. Simeone. *Primary radiation damage in materials: Review of current understanding and proposed new standard displacement damage model to incorporate in-cascade mixing and defect production efficiency effects*. Paris, France: OECD Nuclear Energy Agency, 2015.
- [32] G. S. Was. *Fundamentals of radiation materials science: metals and alloys*. Springer, 2016, pp. 75–77.
- [33] G. A. El-Awadi, S. Abdel-Samad, and E. S. Elshazly. “Hot corrosion behavior of Ni based Inconel 617 and Inconel 738 superalloys”. *Applied surface science* 378 (2016).
- [34] B. Cantor, I. T. H. Chang, P. Knight, and A. J. B. Vincent. “Microstructural development in equiatomic multicomponent alloys”. *Materials Science and Engineering: A* 375–377 (2004).

- [35] J.-W. Yeh, S.-K. Chen, S.-J. Lin, J.-Y. Gan, T.-S. Chin, T.-T. Shun, C.-H. Tsau, and S.-Y. Chang. “Nanostructured high-entropy alloys with multiple principal elements: novel alloy design concepts and outcomes”. *Advanced Engineering Materials* 6.5 (2004).
- [36] M. Harper et al. “python-ternary: Ternary Plots in Python”. *Zenodo 10.5281/zenodo.594435* (2015).
- [37] B. S. Murty, J.-W. Yeh, S. Ranganathan, and P. P. Bhattacharjee. *High-entropy alloys*. Elsevier, 2019.
- [38] J.-W. Yeh. “Recent progress in high entropy alloys”. *Annales de Chimie Science des Matériaux* 31.6 (2006).
- [39] M. H. Tsai and J.-W. Yeh. “High-Entropy Alloys: A Critical Review”. *Materials Research Letters* 2.3 (2014).
- [40] Y. F. Ye, Q. Wang, J. Lu, C. T. Liu, and Y. Yang. “High-entropy alloy: challenges and prospects”. *Materials Today* 19.6 (2016).
- [41] C.-Y. Hsu, T.-S. Sheu, J.-W. Yeh, and S.-K. Chen. “Effect of iron content on wear behavior of $\text{AlCoCrFe}_x\text{Mo}_{0.5}\text{Ni}$ high-entropy alloys”. *Wear* 268.5-6 (2010).
- [42] S. Guo and C. T. Liu. “Phase stability in high entropy alloys: Formation of solid-solution phase or amorphous phase”. *Progress in Natural Science: Materials International* 21.6 (2011).
- [43] S. Q. Xia, X. Yang, T. F. Yang, S. Liu, and Y. Zhang. “Irradiation Resistance in $\text{Al}_x\text{CoCrFeNi}$ High Entropy Alloys”. *The Journal of The Minerals, Metals & Materials Society* 67.10 (2015).
- [44] N. A. P. K. Kumar, C Li, K. J. Leonard, H. Bei, and S. J. Zinkle. “Microstructural stability and mechanical behavior of FeNiMnCr high entropy alloy under ion irradiation”. *Acta Materialia* 113 (2016).
- [45] F. Granberg, F. Djurabekova, E. Levo, and K. Nordlund. “Damage buildup and edge dislocation mobility in equiatomic multi-component alloys”. *Nuclear Instruments and Methods in Physics Research Section B* 393 (2017).
- [46] O. El-Atwani, N. Li, M. Li, A. Devaraj, J. K. S. Baldwin, M. M. Schneider, D. Sobieraj, J. S. Wróbel, D. Nguyen-Manh, S. A. Maloy, et al. “Outstanding radiation resistance of tungsten-based high-entropy alloys”. *Science advances* 5.3 (2019).

- [47] D. B. Miracle and O. N. Senkov. “A critical review of high entropy alloys and related concepts”. *Acta Materialia* 122 (2017).
- [48] W. H. Liu, Y. Wu, J. Y. He, T. G. Nieh, and Z. P. Lu. “Grain growth and the Hall–Petch relationship in a high-entropy Fe–CrNiCoMn alloy”. *Scripta Materialia* 68.7 (2013).
- [49] M. P. Allen and D. J. Tildesley. *Computer simulation of liquids*. Oxford university press, 2017.
- [50] C. W. Gear. “Numerical initial value problems in ordinary differential equations”. *Prentice-Hall series in automatic computation* (1971).
- [51] K. Nordlund, M. Ghaly, R. S. Averback, M. Caturla, T. Diaz de la Rubia, and J. Tarus. “Defect production in collision cascades in elemental semiconductors and FCC metals”. *Physical Review B* 57.13 (1998).
- [52] M. Ghaly, K. Nordlund, and R. S. Averback. “Molecular dynamics investigations of surface damage produced by kiloelectronvolt self-bombardment of solids”. *Philosophical Magazine A* 79.4 (1999).
- [53] H. J. C. Berendsen, J. P. M. Postma, W. F. van Gunsteren, A. DiNola, and J. R. Haak. “Molecular dynamics with coupling to external bath”. *The Journal of Chemical Physics* 81.8 (1984).
- [54] K. Nordlund. “Molecular dynamics simulation of ion ranges in the 1–100 keV energy range”. *Computational materials science* 3.4 (1995).
- [55] M. R. Gilbert, J. Marian, and J.-C. Sublet. “Energy spectra of primary knock-on atoms under neutron irradiation”. *Journal of nuclear materials* 467 (2015).
- [56] M. S. Daw, S. M. Foiles, and M. I. Baskes. “The embedded-atom method: a review of theory and applications”. *Materials Science Reports* 9.7 (1993).
- [57] M.-C. Marinica, L. Ventelon, M. R. Gilbert, L. Proville, S. L. Dudarev, J. Marian, G. Bencteux, and F. Willaime. “Interatomic potentials for modelling radiation defects and dislocations in tungsten”. *Journal of Physics: Condensed Matter* 25.39 (2013).
- [58] M. S. Daw and M. I. Baskes. “Embedded-atom method: Derivation and application to impurities, surfaces, and other defects in metals”. *Physical Review B* 29.12 (1984).

- [59] J. F. Ziegler, J. P. Biersack, and U. Littmark. *The Stopping and Range of Ions in Matter*. New York: Pergamon, 1985.
- [60] J. Byggmästar, F. Granberg, and K. Nordlund. “Effects of the short-range repulsive potential on cascade damage in iron”. *Journal of Nuclear Materials* 508 (2018).
- [61] X. W. Zhou, R. A. Johnson, and H. N. G. Wadley. “Misfit-energy-increasing dislocations in vapor-deposited CoFe/NiFe multilayers”. *Physical Review B* 69 (2004).
- [62] Z. Lin, R. A. Johnson, and L. V. Zhigilei. “Computational study of the generation of crystal defects in a bcc metal target irradiated by short laser pulses”. *Physical Review B* 77.214108 (2008).
- [63] G. Bonny, N. Castin, and D. Terentyev. “Interatomic potential for studying ageing under irradiation in stainless steels: the FeNiCr model alloy”. *Modelling and Simulation in Materials Science and Engineering* 21.8 (2013).
- [64] G. P. Purja Pun, V. Yamakov, and Y. Mishin. “Interatomic potential for the ternary Ni-Al-Co system and application to atomistic modeling of the B2-L1₀ martensitic transformation”. *Modelling and Simulation in Materials Science and Engineering* 23.6 (2015).
- [65] A. E. Sand, K. Nordlund, and S. L. Dudarev. “Radiation damage production in massive cascades initiated by fusion neutrons in tungsten”. *Journal of Nuclear Materials* 455.1-3 (2014).
- [66] F. Granberg, J. Byggmästar, and K. Nordlund. “Molecular dynamics simulations of high-dose damage production and defect evolution in tungsten”. *Journal of Nuclear Materials* 556 (2021).
- [67] J. Behler. “Perspective: Machine learning potentials for atomistic simulations”. *The Journal of chemical physics* 145.17 (2016).
- [68] J. Byggmästar, A. Hamedani, K. Nordlund, and F. Djurabekova. “Machine-learning interatomic potential for radiation damage and defects in tungsten”. *Physical Review B* 100.14 (2019).
- [69] A. Stukowski. “Visualization and analysis of atomistic simulation data with OVITO-the Open Visualization Tool”. *Modelling and Simulation in Materials Science and Engineering* 18.1 (2010).
- [70] E. Wigner and F. Seitz. “On the constitution of metallic sodium”. *Physical Review* 43.10 (1933).

- [71] A. Stukowski, V. V. Bulatov, and A. Arsenlis. “Automated identification and indexing of dislocations in crystal interfaces”. *Modelling and Simulation in Materials Science and Engineering* 20.8 (2012).
- [72] J. D. Honeycutt and H. C. Andersen. “Molecular dynamics study of melting and freezing of small Lennard-Jones clusters”. *Journal of Physical Chemistry* 91.19 (1987).
- [73] D. Faken and H. Jónsson. “Systematic analysis of local atomic structure combined with 3D computer graphics”. *Computational Materials Science* 2.2 (1994).
- [74] A. Stukowski. “Structure identification methods for atomistic simulations of crystalline materials”. *Modelling and Simulation in Materials Science and Engineering* 20.4 (2012).
- [75] S. Zhang, K. Nordlund, F. Djurabekova, Y. Zhang, G. Velisa, and T. S. Wang. “Simulation of Rutherford backscattering spectrometry from arbitrary atom structures”. *Physical Review E* 94.4 (2016).
- [76] X. Jin, J.-P. Crocombette, F. Djurabekova, S. Zhang, K. Nordlund, F. Garrido, and A. Debelle. “New developments in the simulation of Rutherford backscattering spectrometry in channeling mode using arbitrary atom structures”. *Modelling and Simulation in Materials Science and Engineering* 28.7 (2020).
- [77] S. Zhang, K. Nordlund, F. Djurabekova, F. Granberg, Y. Zhang, and T. S. Wang. “Radiation damage buildup by athermal defect reactions in nickel and concentrated nickel alloys”. *Materials Research Letters* 5.6 (2017).
- [78] G. Voronoi. “Nouvelles applications des paramètres continus à la théorie des formes quadratiques. Premier mémoire. Sur quelques propriétés des formes quadratiques positives parfaites.” *Journal für die reine und angewandte Mathematik*. 1908.133 (1908).
- [79] G. Voronoi. “Nouvelles applications des paramètres continus à la théorie des formes quadratiques. Deuxième mémoire. Recherches sur les paralléloèdres primitifs.” *Journal für die reine und angewandte Mathematik*. 1908.134 (1908).
- [80] G. Voronoi. “Nouvelles applications des paramètres continus à théorie des formes quadratiques. Deuxième Mémoire. Recherches sur les paralléloèdres primitifs.” *Journal für die reine und angewandte Mathematik*. 1909.136 (1909).

- [81] E. Levo, F. Granberg, C. Fridlund, K. Nordlund, and F. Djurabekova. “Radiation damage buildup and dislocation evolution in Ni and equiatomic multicomponent Ni-based alloys”. *Journal of Nuclear Materials* 490 (2017).
- [82] E. Levo, F. Granberg, K. Nordlund, and F. Djurabekova. “Temperature effect on irradiation damage in equiatomic multi-component alloys”. *Computational Materials Science* 197 (2021).
- [83] E. Levo, F. Granberg, D. Utt, K. Albe, K. Nordlund, and F. Djurabekova. “Radiation stability of nanocrystalline single-phase multicomponent alloys”. *Journal of Materials Research* 34.5 (2019).